different multiplicities of infection (MOIs) in A549 cells with CalcuSyn software (BioSoft, Cambridge, UK).

Cell cycle analysis

A549 and MKN45 cells were seeded on 6-well plates at 1×10^5 cells/well and were infected with OBP-301 at an MOI of 1 PFU/cell, Ad/Bax at an MOI of 5 or 50 PFU/cell, or OBP-301 at an MOI of 1 PFU/cell in combination with Ad/Bax at an MOI of 5 PFU/cell 15 hr later. At 24 and 96 hr after infection, adherent cells were harvested with trypsin-EDTA and nonadherent cells were also harvested. All cells were washed with PBS, fixed and permeated with 70% ice-cold ethanol at 4°C for 12 h. Cells were centrifuged at 1,200 rpm, resuspended in freshly prepared propidium iodide (PI) staining buffer (0.1% Triton X-100, 200 μg/ml RNase, and 50 μg/ml PI in PBS), and incubated for 30 min at 4°C in the dark. Single color fluorescent flow cytometry was performed with a FACS calibur flow cytometer (Becton Dickinson, San Jose, CA). The histograms were analyzed with FlowJO software (Tree Star, Ashland, OR).

Western blot analysis

A549 cells were seeded and infected with OBP-301 alone, Ad/Bax alone, or their combination at an MOI of 1 PFU/cell 15 hr later. The cells were incubated at 37°C and harvested for Western blot analysis at 72 and 120 hr. The primary antibodies against Bax (Santa Cruz Biotechnology, Santa Cruz, CA), caspase 3, E1A (BD Biosciences, San Jose, CA) and β-actin (Sigma, St. Louis, MO) and peroxidase-linked secondary antibody (Amersham, Arlington Heights IL) were used. Cells were washed twice in cold PBS, collected and lysed in lysis buffer [10 mM Tris (pH 7.5), 150 mM NaCl, 50 mM NaF, 1 mM EDTA, 10% glycerol, 0.5% NP40] containing proteinase inhibitors (0.1 mM phenylmethylsulfonyl fluoride, 0.5 mM Na3VO4). After 20 min on ice, the lysates were spun at 14,000 rpm at 4°C for 10 min. The supernatants were used as whole cell extracts. Protein concentration was determined using the Bio-Rad protein determination method (Bio-Rad, Richmond, CA). Equal amounts of proteins were boiled for 5 min and electrophoresed under reducing conditions on 4–12% (w/v) polyacrylamide gels. Proteins were electrophoretically transferred to Hybond polyvinylidene difluoride transfer membranes (Amersham Life Science, Buckinghamshire, UK) and incubated with the primary followed by peroxidase-linked secondary antibody. An ECL chemiluminescent Western blot system (Amersham) was used to detect secondary probes.

Animal experiments

A549 xenografts were established in 6-week-old female nude mice (Balb/c nu/nu) through subcutaneous inoculation of 2×10^6 A549 cells into the dorsal flank. Once each tumor reached a diameter of ~3–9 mm, the mice were randomly assigned into 4 groups and a 50-μl solution containing OBP-301, Ad/Bax, or their combination, at a dose of 1×10^7 PFU/body or PBS was injected into the tumor on 3 consecutive days. Tumors were measured 2–3 times a week and tumor volume was calculated using the equation $a \times b^2 \times 0.5$, in which a and b are the largest and smallest diameters, respectively. Animals were killed when their tumor reached a diameter of ~15 mm. To develop pleural disseminated xenografts, mice were inoculated with 2×10^6 A549 cells into the pleural cavity through a 27-gauge needle. Also, to assess the efficiency of adenoviral gene transfer into the pleural disseminated tumors, 24 hr after tumor injection, 100 μl of 1.0×10^7 PFU of OBP-301, Ad/Bax, both of them, or PBS was injected into the thoracic space by the same technique. The procedure was repeated over 3 consecutive days. Three weeks after cell inoculation, the mice were killed and their thoracic spaces were examined macroscopically for any growths. Tumors in the thoracic spaces were removed and weighed. The experimental protocol was approved by the Ethics Review Committee for Animal Experimentation of Okayama University School of Medicine, Okayama, Japan. The tumor growth of each group was statistically analyzed by Student t-test and a p-value of ≤ 0.05 was considered significant.

Viral replication assay in vivo

A549 cells were injected into the dorsal flank of nude mice. When the tumor reached a size of ~5 mm, 1×10^7 PFU of OBP-301, OBP-301 + Ad/Bax, OBP-301 + Ad/LacZ, or Ad/Bax was injected to the tumors ($n = 5$, each group). Tumors were harvested 7 days after viral injection, immediately frozen and milled in PBS by using Micro Smash MS-100 (Tomy Digital Biology, Tokyo, Japan). The virus was then extracted by freezing and thawing 3 times and cell debris was spun down. The supernatant was collected and subjected to titer assay for viral PFU. The final result was expressed as a total PFU from 1 whole tumor.

Quantitative real-time polymerase chain reaction

A549 cells were seeded on 25-cm^2 flasks at 5×10^5 cells 15 hr before infection. Cells were infected with OBP-301 alone or in combination with Ad/Bax or Ad/lacZ 15 hr later. The cells were incubated at 37°C, trypsinized and harvested for replication analysis at 48 hr. DNA purification was performed using a QIAmp DNA mini kit (Qiagen, Valencia, CA). The E1A DNA copy number was determined by quantitative real time polymerase chain reaction (PCR), using a LightCycler instrument and LightCycler-DNA Master SYBR Green I (Roche Diagnostics).

Results

Combination of oncolytic virotherapy and Bax gene therapy enhanced cell killing in vitro

To compare the efficacy of the combined use of oncolytic virotherapy with Bax gene therapy *in vitro*, A549 and MKN45 human cancer cells were treated with OBP-301 alone, Ad/Bax alone, or the combination. Based on each optimal condition, A549 was infected with OBP-301 at 1 MOI and Ad/Bax at 10 MOI, and MKN45 was infected at 10 MOI in both viruses. In both cell lines, Ad/Bax treatment showed only minimal suppression of cell viability and OBP-301 treatment showed a modest and delayed oncolytic effect, whereas combination treatment with OBP-301 and Ad/Bax induced rapid and massive cell death, and almost complete cell killing (Fig. 1).

To evaluate the synergistic effect of the combined oncolytic virotherapy and Bax gene therapy, the CI was determined at different MOIs (Table I) with CalcuSyn software (BioSoft, Cambridge, UK). We found that in A549 cells, the combination of OBP-301 with Ad/Bax led to a strong synergism ($CI < 0.3$).

Bax gene therapy in combination with oncolytic virotherapy increased the production of Bax protein in vitro *and induction of apoptosis*

To examine Bax protein expression in cells infected with the replication-deficient Ad/Bax in combination with the replicating OBP-301, A549 cells were infected with OBP-301 alone, Ad/Bax alone, or OBP-301 in combination with Ad/Bax or Ad/lacZ and then harvested on day 3 or 5. Cells treated with OBP-301 or the combination of OBP-301 with Ad/lacZ resulted in minimal Bax protein expression, whereas treatment with Ad/Bax and the combination treatment with OBP-301 plus Ad/Bax showed higher expression of Bax protein. Densitometric measurement documented increments of Bax expression by combination of Ad/Bax with OBP-301 (Fig. 2). In addition, treatment with OBP-301 plus Ad/Bax resulted in caspase-3 activation, while treatment with OBP-301 only or OBP-301 plus control virus Ad/lacZ did not. This means that the combination with Ad/Bax activates the apoptotic cascade in cancer cells cotreated with oncolytic virus.

Bax gene therapy in combination with oncolytic virotherapy increased apoptotic cells in vitro

To quantify the apoptotic effects of Ad/Bax treatment in combination with OBP-301 treatment, sub-G1/G0 fractions were

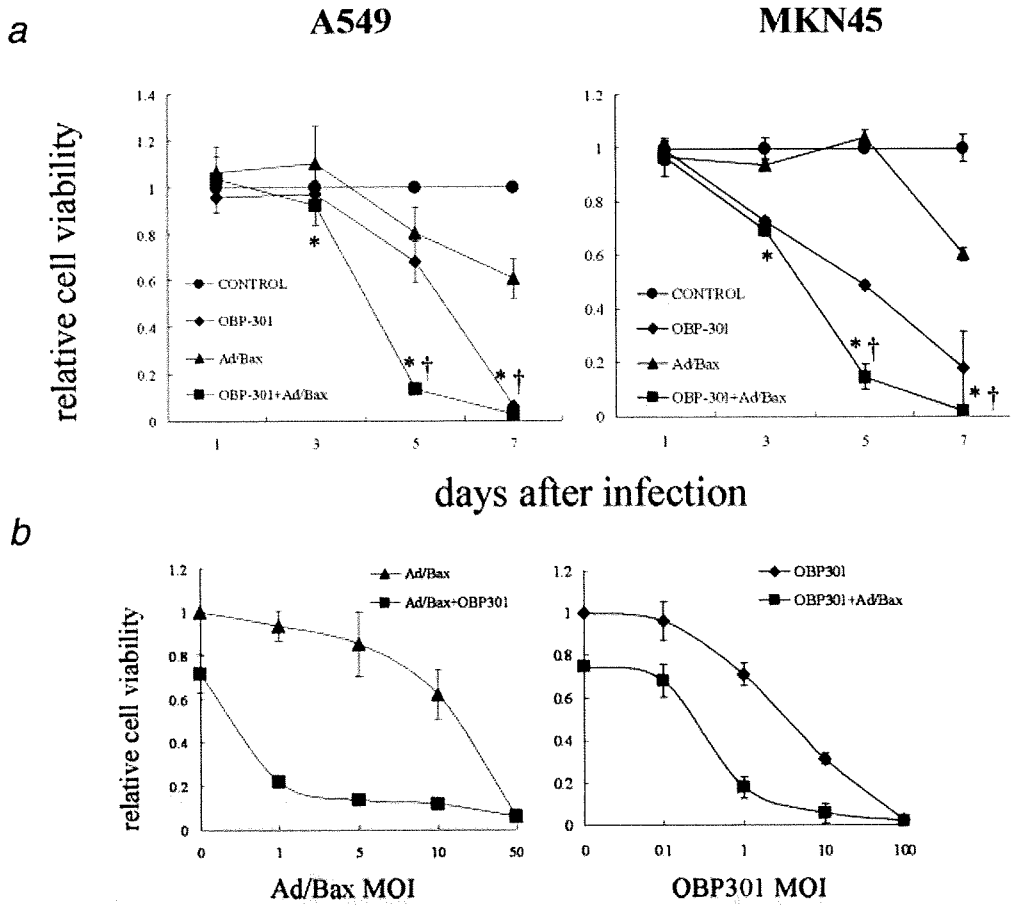

FIGURE 1 – Cytotoxity effects of OBP-301 combined with Ad/Bax in human cancer cell lines. (*a*) The indicated cancer cells were infected with OBP-301 alone, Ad/Bax alone, or in combination at the indicated MOI. Cell viability was assessed by XTT assay over 7 days. Bars, standard deviation (SD). *, $p < 0.05$, OBP-301 + Ad/Bax versus Ad/Bax alone; †, $p < 0.05$, OBP-301 + Ad/Bax versus OBP-301 alone. (*b*) A549 cells were infected with 1 MOI of OBP-301 and Ad/Bax at the indicated MOI (left), or 10 MOI of Ad/Bax and OBP-301 at the indicated MOI (right). Cell viability was assessed by XTT assay at 5 days after infection. Bars, SD.

TABLE 1 – COMBINATION INDEX (CI) OF OBP-301 AND Ad/Bax

Ad/Bax (MOI)	CI
1	0.122
5	0.111
10	0.132
50	0.217
OBP301 (MOI)	**CI**
0.1	1.054
1	0.144
10	0.197
100	0.592

determined by flow cytometry. A549 cells were infected with OBP-301, Ad/Bax, or OBP-301 plus Ad/Bax, and then subjected to the analysis at day 4. Although treatment with OBP-301 or Ad/Bax resulted in only background levels of apoptotic cells similar to that of mock infection, treatment with Ad/Bax plus OBP-301 markedly increased the apoptotic cells (Fig. 3).

Combination with Bax gene therapy did not augment antitumor activity of OBP-301-mediated oncolytic virotherapy in vivo

Based on the *in vitro* favorable combination effect of Ad/Bax and OBP-301, the antitumor effect on established tumors was further assessed. The A549 tumors were established in the dorsal

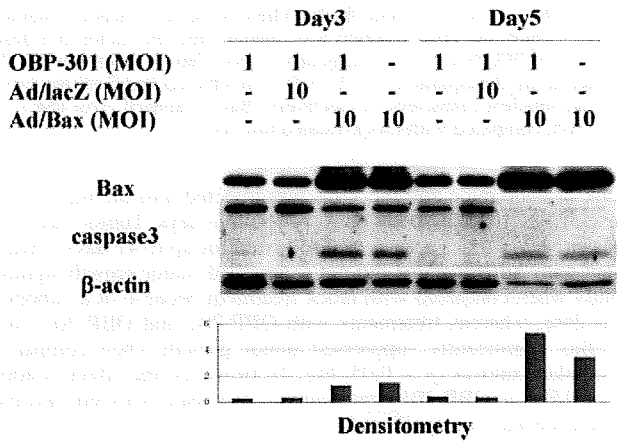

FIGURE 2 – Expression of Bax and caspase 3 in cells infected with Ad/Bax in combination with OBP-301. A549 cells were infected at 1 MOI of OBP-301 alone, 10 MOI of Ad/Bax alone, or 1 MOI of OBP-301 in combination with 10 MOI of Ad/Bax or Ad/lacZ, and then harvested at day 3 or 5. Lysates were subjected to immunoblot analysis with antibodies recognizing Bax, caspase 3, or β-actin. The lower panel shows the intensity of each band of Bax determined by densitometric scanning using NIH image software and normalized by dividing the actin signal.

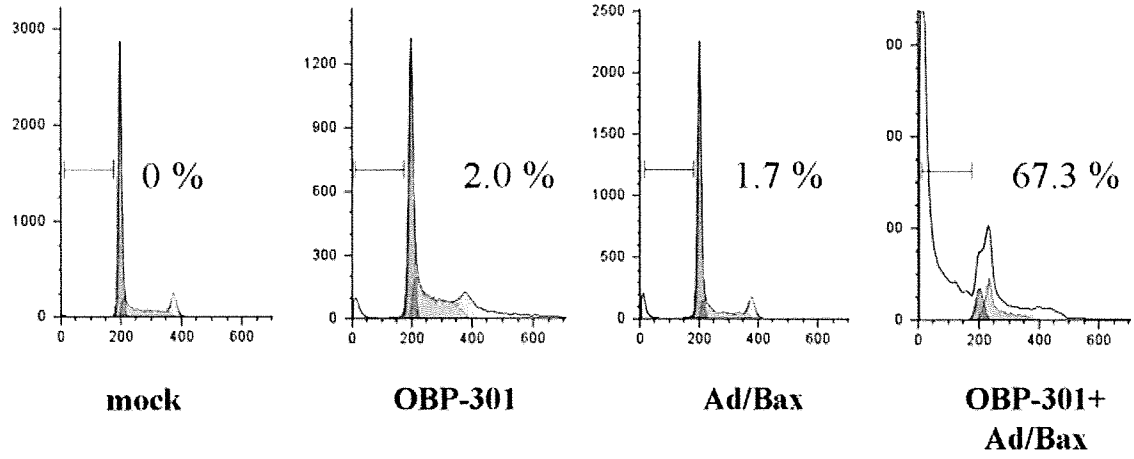

FIGURE 3 – Cell cycle analysis in A549 cells infected with OBP-301 in combination with Ad/Bax. Indicated cancer cells were infected with mock solution, 1 MOI of OBP-301, 10 MOI of Ad/Bax, or 1 MOI of OBP-301 plus 10 MOI of Ad/Bax, and harvested at day 4; cell cycle analysis using flow cytometry was then performed. The histograms were analyzed with FlowJO software.

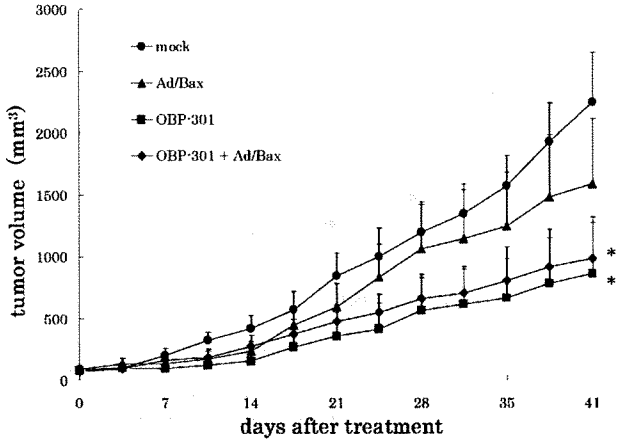

FIGURE 4 – Tumor xenograft size after infection with OBP-301, Ad/Bax, or their combination. A549 xenografts were established in nude mice (Balb/c nu/nu) through subcutaneous inoculation of 2×10^6 A549 cells into the dorsal flank. When the tumor reached a diameter of ~5 mm, the virus solution was injected into the tumor at a dose of 1×10^7 PFU/body on 3 consecutive days. Tumor volume was calculated using the equation $a \times b^2 \times 0.5$, in which a and b are the largest and smallest diameters, respectively. Bars, standard error (SE). *, $p < 0.05$, compared with mock-treated tumors.

flank of nude mice and the virus was injected into the tumor at a dose of 1×10^7 PFU/body on 3 consecutive days. Tumor size was measured 2–3 times a week and followed for up to 41 days. Treatment with Ad/Bax alone did not suppressed tumor growth significantly when compared with mock treatment because of a suboptimal dose, whereas treatments with OBP-301 and OBP-301 plus Ad/Bax significantly suppressed tumor growth when compared with other controls ($p \leq 0.05$; Fig. 4). However, the effect of adding Ad/Bax to OBP-301 treatment was less than expected, and the difference was not significant.

We also examined the antitumor effects of this combination treatment in mice with pleurally disseminated A549 tumors. The mice were injected with 100 µl of 1.0×10^7 PFU of OBP-301, Ad/Bax, or both into the thoracic space on 3 consecutive days. Three weeks after cell inoculation, the mice were killed and their thoracic spaces were examined macroscopically for any growths. To quantitate the reduction of tumor burden in the thoracic spaces, the tumors were removed and weighed. Although treatment with OBP-301 alone or Ad/Bax in combination with OBP-301 significantly suppressed tumor weight, there was no significant difference between them (Figs. 5*a* and 5*b*). These results suggest that Bax gene therapy does not augment oncolytic virotherapy *in vivo*.

Combination treatment resulted in suppressed E1A protein expression due to reduced viral replication in vitro

To explore the underlying mechanism by which oncolytic virotherapy did not work cooperatively with proapoptotic Bax gene therapy, E1A protein expression was examined by Western blot analysis. A549 cells were treated with each virus singly or in combination and then subjected to the analysis at days 3 and 5. Treatment with OBP-301 alone and in combination treatment with Ad/lacZ demonstrated increased E1A protein expression, meaning efficient viral replication. Treatment with Ad/Bax alone showed no E1A protein expression because of the E1-deficient replication incompetent virus. Of note, treatment with OBP-301 plus Ad/Bax showed suppressed expression of E1A protein when compared with treatment with OBP-301 alone, meaning that the combination with Ad/Bax may interfere with viral replication (Fig. 6).

To further document the effect of Bax expression on the process of viral propagation, the replication and release of viral progenies were measured by quantitative real time PCR. A549 cells were infected with viruses and the supernatants of the cell groups were collected. DNA was extracted from them and subjected to the assay. We found suppressed viral copy numbers in cells treated with the combinations with Ad/Bax and Ad/lacZ (Fig. 7). The inhibition of E1A copy numbers in a group of Ad/Bax combination was about 10 times of inhibition in a group of Ad/lacZ combination. Our results suggest that Bax gene therapy may interfere with viral production and thus be not conducive to oncolytic virotherapy. To further examine viral replication *in vivo*, the amounts of infectious viruses produced in the tumors were analyzed. Titers were very low for tumors treated with Ad/Bax because of a lack of replication in the absence of E1 gene, while tumors treated with OBP-301 produced higher amount of infectious virus than those treated with Ad/Bax alone, suggesting viral replication in tumors. However, because of the large variation in data from each group, there was no significant difference between treatment groups (data not shown).

Discussion

Replication-competent oncolytic adenovirus has shown a remarkable safety profile but efficacy for cancer therapy continues to be a major obstacle. To eliminate cancer cells, the virus also must spread throughout the bulk of the tumor and induce cell

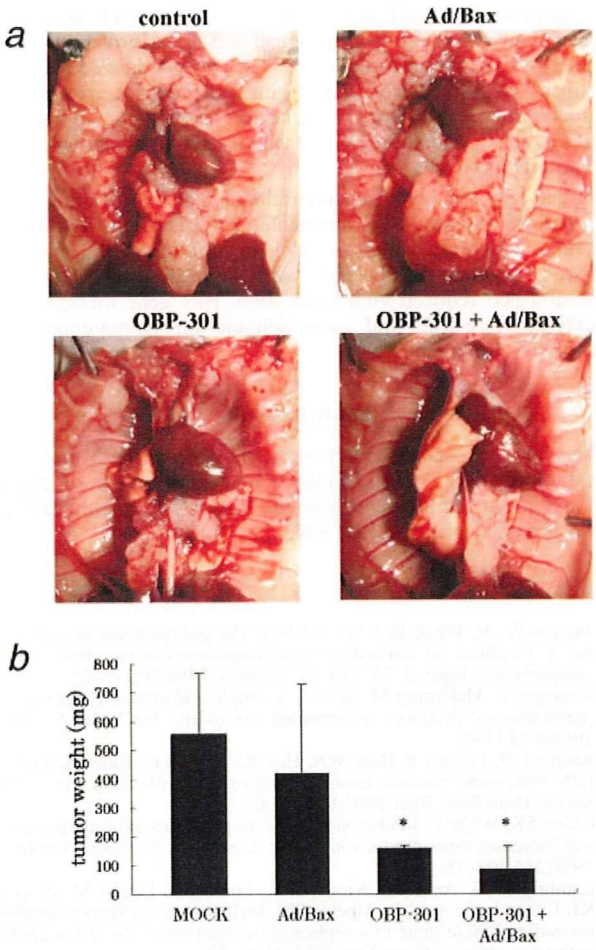

FIGURE 5 – Antitumor effects of OBP-301 combined with Ad/Bax in mice with A549 pleural dissemination. Mice were inoculated with 2×10^6 A549 cells into the pleural cavity, and 24 hr after tumor injection, 100 μl of 1.0×10^7 PFU of OBP-301, Ad/Bax, both of them, or PBS was injected into the thoracic space. The procedure was repeated over 3 consecutive days. (*a*) Three weeks after cell inoculation, mice were killed and their thoracic spaces were examined macroscopically for any growths. (*b*) Tumors in the thoracic spaces were removed and weighed. Bars, SD. *, $p < 0.05$, compared with mock-treated tumors.

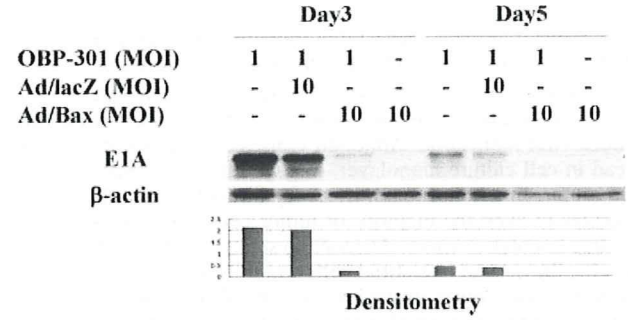

FIGURE 6 – Expression of E1A in cells infected with Ad/Bax in combination with OBP-301. A549 cells were infected at 1 MOI of OBP-301 alone, 10 MOI of Ad/Bax alone, or 1 MOI of OBP-301 in combination with 10 MOI of Ad/Bax or Ad/lacZ, and then harvested at day 3 or 5. Lysates were subjected to immunoblot analysis with antibodies recognizing E1A or β-actin. The lower panel shows the intensity of each band of Bax determined by densitometric scanning using NIH image software and normalized by dividing the actin signal.

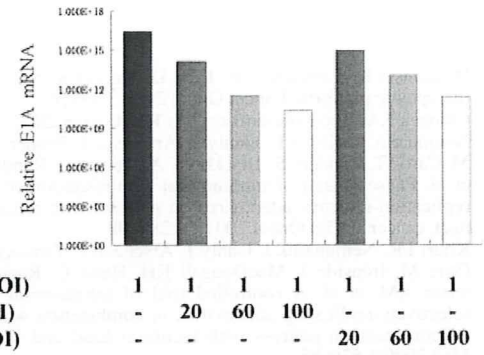

FIGURE 7 – Assessment of viral DNA replication in cells infected with Ad/Bax in combination with OBP-301. A549 cells were seeded on 25-cm^2 flasks at 5×10^5 cells 15 hr before infection. Cells were infected with OBP-301 alone, Ad/Bax alone, or their combination at an MOI of 1 PFU/cell 15 hr later. The cells were harvested at 48 hr and then subjected to real-time quantitative PCR assay. The amounts of viral E1A copy number are defined as the fold increase for each sample relative to that at 2 hr (2 hr equals 1).

death. Even with replicating adenoviral systems, the necessity to infect all cancer cells remains a major challenge.

In this study, we hypothesized that the oncolytic adenovirotherapy combined with Bax gene therapy could enhance the oncolytic potency. As expected, the combination treatment resulted in Bax overexpression, induced early apoptosis and enhanced efficacy in the cell viability assay *in vitro*. However, disappointingly, combination treatment did not result in further reductions in flank tumor size and pleural disseminated tumor weight, which was associated with suppressed E1A protein expression and reduced viral replication of OBP-301.

The antitumor effect of the oncolytic virus depends on the cytopathic effect intrinsic to adenovirus replication and dissemination throughout the tumor mass. Because viral infection of the tumor bulk depends on cell-to-cell viral spread, there may be a race between rapid tumor growth and viral spread. Therefore, to improve the efficacy of oncolytic virotherapy, the accelerated viral release and induction of cell death must be necessary. A previous study has shown that loss of E1b-19kD function in a replicating adenovirus enhances early viral release, leading to accelerated cell-to-cell viral spread.[17] In turn, Chiou and White reported that inhibition of apoptosis could severely attenuate viral release.[18] Taken together, this suggests that a combination of proapoptotic gene therapy and oncolytic virotherapy may improve the antitumor efficacy by enhancing cell-to-cell spread of the virus. The other rationale of the combination of proapoptotic gene therapy is to cope with the cancer resistance to the oncolytic virotherapy. Because heterogeneity in cancer cell populations drives the development of resistance, the approach of killing cells by multiple nonoverlapping mechanisms could be a solution. Although an oncolytic virus can kill cells by apoptosis-independent mechanisms such as direct cell lysis and necrosis, cells treated with combination therapy showed a pattern of apoptosis evidenced by analysis of the cell cycle. However, because induction of apoptosis and premature cell lysis may potentially compromise viral yield, reduced viral production could be a concern in using Bax-expressing virus in combination.

In the *in vitro* cell viability assay, the combination of Bax-expressing adenovirus with a replicating adenovirus leads to increased apoptosis at an earlier phase as theoretically anticipated. In turn, we have demonstrated a reduced viral yield in A549 cells. The early apoptotic cell death induced by Bax overexpression may limit an increase of virus and disturb viral replication. Our results are consistent with those of Lambright *et al.*,[19] who found that the addition of ganciclovir therapy to a replicating vector containing the HSVtk suicide gene did not augment efficacy, despite the enhanced production of the transgene. Viral replication and timely cell-death induction thus need to be well coordinated, and forced

induction of early apoptosis could be a cause of losing the combinative effect. Our data suggest that impaired viral replication may offset the benefits due to enhanced transgene spread *in vivo*.

In this study, we have shown the discrepancy between *in vitro* and *in vivo* findings, but this would not result solely from the reduced viral replication. Although viruses can rapidly and evenly spread in cell culture monolayer, this would not be expected in a solid tumor. In a tumor mass, it is very difficult to distribute viral progenies to even the majority of tumor cells. Because a cancer-targeting oncolytic virus is designed to selectively replicate in cancer cells, the normal interstitial cells would be obstacles. The virus would also face other obstacles for viral distribution, including tight intercellular space and continuous drainage by the circulatory and lymphatic systems. In this circumstance, the intratumoral dispersion is confined to one part of the tumor, and thus the requirement of double infection in a complementary strategy curtails the efficacy at low multiplicities of infection.

Although our data suggest that Bax gene therapy in combination with oncolytic adenovirotherapy is not likely to be therapeutically beneficial, the concept of "armed" replicating adenovirotherapy still has potential merit. Overexpression of the adenoviral death protein, expression of TRAIL and deletion of the E1B-19kD gene have all been shown to improve viral spread and efficacy of replicating adenoviruses *in vitro* and *in vivo*.[5,17,20–25] Various suicide genes or cytokines have also been expressed with replication-competent vectors to improve cell killing.[26–30] One important factor to keep in mind is to enhance antitumor effect without inhibiting the proliferative capacity of viruses.

In summary, oncolytic adenovirotherapy in combination with Bax gene therapy resulted in augmented cell killing *in vitro*. However, in a xenografted tumor model, oncolytic efficacy was not improved; this was associated with suppressed E1A protein expression and reduced viral replication. Bax gene therapy may possibly interfere with viral production and thus be not conducive to oncolytic virotherapy.

Acknowledgements

This work was supported in part by grants from the Ministry of Education, Culture, Sports, Science and Technology of Japan (T.F. and S.K.); and by grants from the Ministry of Health, Labour and Welfare of Japan (T.F. and S.K.).

References

1. Hawkins LK, Lemoine NR, Kirn D. Oncolytic biotherapy: a novel therapeutic platform. Lancet Oncol 2002;3:17–26.
2. Chiocca EA. Oncolytic viruses. Nat Rev Cancer 2002;2:938–50.
3. Nemunaitis J, Khuri F, Ganly I, Arseneau J, Posner M, Vokes EK, McCarty T, Landers S, Blackburn A, Romel L, Randlev B, Kaye S, et al. Phase II trial of intratumoral administration of ONYX-015, a replication-selective adenovirus, in patients with refractory head and neck cancer. J Clin Oncol 2001;19:289–98.
4. Khuri FR, Nemunaitis J, Ganly I, Arseneau J, Tannock IF, Romel L, Gore M, Ironside J, MacDougall RH, Heise C, Randlev B, Gillenwater AM, et al. A controlled trial of intratumoral ONYX-015, a selectively-replicating adenovirus, in combination with cisplatin and 5-fluorouracil in patients with recurrent head and neck cancer. Nat Med 2000;6:879–85.
5. Harrison D, Sauthoff H, Heitner S, Jagirdar J, Rom W, Hay J. Wild-type adenovirus decreases tumor xenograft growth, but despite viral persistence complete tumor responses are rarely achieved-deletion of the viral E1b-19kDa gene increases the oncolytic effect. Hum Gene Ther 2001;12:1323–32.
6. DeWeese TL, van der Poel H, Li S, Mikhak B, Drew R, Goemann M, Hamper U, DeJong R, Detorie N, Rodriguez R, Haulk T, DeMarzo AM, et al. A phase I trial of CV706, a replication-competent, PSA selective oncolytic adenovirus, for the treatment of locally recurrent prostate cancer following radiation therapy. Cancer Res 2001;61:7464–72.
7. Reid T, Galanis E, Abbruzzese J, Sze D, Wein LM, Andrews J, Randlev B, Heise C, Uprichard M, Hatfield M, Rome L, Rubin J, et al. Hepatic arterial infusion of a replication-selective oncolytic adenovirus (dl1520): phase II viral, immunologic, and clinical endpoints, Cancer Res 2002;62:6070–79.
8. Hamid O, Varterasian ML, Wadler S, Hecht JR, Benson A, Galanis E, Uprichard M, Omer C, Bycott P, Hackman RC, Shields AF. Phase II trial of intravenous CI-1042 in patients with metastatic colorectal cancer. J Clin Oncol 2003;21:1498–504.
9. Jurgensmeier JM, Xie Z, Deveraux Q, Ellerby L, Bredesen D, Reed JC. Bax directly induces release of cytochrome c from isolated mitochondria. Proc Natl Acad Sci USA 1998;95:4997–5002.
10. Pastorino JG, Chen ST, Tafani M, Snyder JW, Farber JL. The overexpression of Bax produces cell death upon induction of the mitochondrial permeability transition. J Biol Chem 1998;273:7770–5.
11. Kagawa S, Pearson SA, Ji L, Xu K, McDonnell TJ, Swisher SG, Roth JA, Fang B. A binary adenoviral vector for expressing high levels of the proapoptotic gene bax. Gene Ther 2000;7:75–9.
12. Kagawa S, Gu J, Swisher SG, Ji L, Roth JA, Lai D, Stephens LC, Fang B. Antitumor effect of adenovirus-mediated Bax gene transfer on p53-sensitive and p53-resistant cancer lines. Cancer Res 2000;60:1157–61.
13. Tsunemitsu Y, Kagawa S, Tokunaga N, Otani S, Umeoka T, Roth JA, Fang B, Tanaka N, Fujiwara T. Molecular therapy for peritoneal dissemination of xenotransplanted human MKN-45 gastric cancer cells with adenovirus mediated Bax gene transfer. Gut 2004;53:554–60.
14. Kawashima T, Kagawa S, Kobayashi N, Shirakiya Y, Umeoka T, Teraishi F, Taki M, Kyo S, Tanaka N, Fujiwara T. Telomerase-specific replication-selective virotherapy for human cancer. Clin Cancer Res 2004;10:285–92.
15. Maizel JV, Jr, White DO, Scharff MD. The polypeptides of adenovirus. I. Evidence for multiple protein components in the virion and a comparison of types 2, 7A, and 12. Virology 1968;36:115–25.
16. Kanegae Y, Makimura M, Saito I. A simple and efficient method for purification of infectious recombinant adenovirus. Jpn J Med Sci Biol 1994;47:157–66.
17. Sauthoff H, Heitner S, Rom WN, Hay JG. Deletion of the adenoviral E1b-19kD gene enhances tumor cell killing of a replicating adenoviral vector. Hum Gene Ther 2000;11:379–88.
18. Chiou SK, White E. Inhibition of ICE-like proteases inhibits apoptosis and increases virus production during adenovirus infection. Virology 1998;244:108–18.
19. Lambright ES, Amin K, Wiewrodt R, Force SD, Lanuti M, Propert KJ, Litzky L, Kaiser LR, Albelda SM. Inclusion of the herpes simplex thymidine kinase gene in a replicating adenovirus does not augment antitumor efficacy. Gene Ther 2001;8:946–53.
20. Liu TC, Hallden G, Wang Y, Brooks G, Francis J, Lemoine N, Kirn D. An E1B-19kDa gene deletion mutant adenovirus demonstrates tumor necrosis factor-enhanced cancer selectivity and enhanced oncolytic potency. Mol Ther 2004;9:786–803.
21. Kim J, Cho JY, Kim JH, Jung KC, Yun CO. Evaluation of E1B gene-attenuated replicating adenoviruses for cancer gene therapy. Cancer Gene Ther 2002;9:725–36.
22. Doronin K, Toth K, Kuppuswamy M, Ward P, Tollefson AE, Wold WS. Tumor-specific, replication-competent adenovirus vectors overexpressing the adenovirus death protein. J Virol 2000;74:6147–55.
23. Sova P, Ren XW, Ni S, Bemt KM, Mi J, Kiviat N, Lieber A. A tumor-targeted and conditionally replicating oncolytic adenovirus vector expressing TRAIL for treatment of liver metastases. Mol Ther 2004;9:496–509.
24. Liu XY, Qiu SB, Zou WG, Pei ZF, Gu JF, Luo CX, Ruan HM, Chen Y, Qi YP, Qian C. Effective gene—virotherapy for complete eradication of tumor mediated by the combination of hTRAIL (TNFSF10) and plasminogen k5. Mol Ther 2005;11:531–41.
25. Ye X, Lu Q, Zhao Y, Ren Z, Ren XW, Qiu QH, Tong Y, Liang M, Hu F, Chen HZ. Conditionally replicative adenovirus vector carrying TRAIL gene for enhanced oncolysis of human hepatocellular carcinoma. Int J Mol Med 2005;16:1179–84.
26. Bristol JA, Zhu M, Ji H, Mina M, Xie Y, Clarke L, Forry-Schaudies S, Ennist DL. In vitro and in vivo activities of an oncolytic adenoviral vector designed to express GM-CSF. Mol Ther 2003;7:755–64.
27. Ramesh N, Ge Y, Ennist DL, Zhu M, Mina M, Ganesh S, Reddy PS, Yu DC. CG0070, a conditionally replicating granulocyte macrophage colony-stimulating factor—armed oncolytic adenovirus for the treatment of bladder cancer. Clin Cancer Res 2006;12:305–13.
28. Zhao L, Gu J, Dong A, Zhang Y, Zhong L, He L, Wang Y, Zhang J, Zhang Z, Huiwang J, Qian Q, Qian C, et al. Potent antitumor activity of oncolytic adenovirus expressing mda-7/IL-24 for colorectal cancer. Hum Gene Ther 2005;16:845–58.
29. Nanda D, Vogels R Havenga M, Avezaat CJ, Bout A, Smitt PS. Treatment of malignant gliomas with a replicating adenoviral vector expressing herpes simplex virus-thymidine kinase. Cancer Res 2001;61:8743–50.
30. Lee CT, Park KH, Yanagisawa K, Adachi Y, Ohm JE, Nadaf S, Dikov MM, Curiel DT, Carbone DP. Combination therapy with conditionally replicating adenovirus and replication defective adenovirus. Cancer Res 2004;64:6660–5.

Gene Therapy (2008) 15, 1233–1239

www.nature.com/gt

SHORT COMMUNICATION

Autophagy-inducing agents augment the antitumor effect of telomerase-selective oncolytic adenovirus OBP-405 on glioblastoma cells

T Yokoyama[1,8], E Iwado[1,8], Y Kondo[1], H Aoki[1], Y Hayashi[2], MM Georgescu[2], R Sawaya[1,3], KR Hess[4], GB Mills[5], H Kawamura[6], Y Hashimoto[6], Y Urata[6], T Fujiwara[6,7] and S Kondo[1,3]

[1]Department of Neurosurgery, The University of Texas MD Anderson Cancer Center, Houston, TX, USA; [2]Department of Neuro–Oncology, The University of Texas MD Anderson Cancer Center, Houston, TX, USA; [3]Department of Neurosurgery, Baylor College of Medicine, Houston, TX, USA; [4]Department of Biostatistics and Applied Mathematics, The University of Texas MD Anderson Cancer Center, Houston, TX, USA; [5]Department of Molecular Therapeutics, The University of Texas MD Anderson Cancer Center, Houston, TX, USA; [6]Oncolys BioPharma Inc., Tokyo, Japan and [7]Division of Surgical Oncology, Department of Surgery, Okayama University Graduate School of Medicine and Dentistry, Okayama, Japan

Oncolytic adenoviruses are a promising tool in cancer therapy. In this study, we characterized the role of autophagy in oncolytic adenovirus-induced therapeutic effects. OBP-405, an oncolytic adenovirus regulated by the human telomerase reverse transcriptase promoter (hTERT-Ad, OBP-301) with a tropism modification (RGD) exhibited a strong antitumor effect on glioblastoma cells. When autophagy was inhibited pharmacologically, the cytotoxicity of OBP-405 was attenuated. In addition, autophagy-deficient Atg5$^{-/-}$ *mouse embryonic fibroblasts (MEFs) were less sensitive than wild-type MEFs to OBP-405. These findings indicate that OBP-405-induced autophagy is a cell killing effect. Moreover, autophagy-inducing therapies (temozolomide and rapamycin) synergistically sensitized tumor cells to OBP-405 by stimulating the autophagic pathway without altering OBP-405 replication. Mice harboring intracranial tumors treated with OBP-405 and temozolomide survived significantly longer than those treated with temozolomide alone, and mice treated with OBP-405 and the rapamycin analog RAD001 survived significantly longer than those treated with RAD001 alone. The observation that autophagy inducers increase OBP-405 antitumor activity suggests a novel strategy for treating patients with glioblastoma.*
Gene Therapy (2008) **15,** 1233–1239; doi:10.1038/gt.2008.98; published online 26 June 2008

Keywords: *autophagy; glioblastoma; OBP-301; OBP-405*

Oncolytic adenoviruses have recently been developed as a novel cancer therapy.[1,2] We have shown that the oncolytic adenovirus regulated by the human telomerase reverse transcriptase promoter (hTERT-Ad) induces nonapoptotic autophagy in glioblastoma cells.[3] However, the molecular machinery underlying autophagy-induced cell death remains unclear.[4–6] Furthermore, the processes determining whether autophagy in cancer cells causes death or acts as a protective mechanism activated during cellular distress are unknown. In this study, we elucidated the therapeutic role of autophagy in hTERT-Ad infection.

The infection efficiency of adenoviral constructs, which are derived from human adenovirus serotype 5, varies widely depending on the cellular expression of the coxsackievirus and adenovirus receptor (CAR).[7] Modification of the adenoviral fiber protein is one approach to overcoming the limitation imposed by this dependence on CAR.[8] A recent study demonstrated the activity of OBP-405, which is an hTERT-Ad with a tropism modification (RGD): OBP-405 had a profound oncolytic effect *in vitro* and *in vivo* on lung and colon cancer cells regardless of the CAR expression level.[9] In addition, for cells with low CAR expression levels, OBP-405 had a higher rate of infection than did OBP-301, an hTERT-Ad that expresses the *E1A* gene under the control of a 455-bp hTERT promoter.[9] The hTERT-Ad that we used previously has a 255-bp hTERT promoter.[3]

Good manufacturing practice OBP-301 (Telomelysin) and OBP-405 (Telomelysin-RGD) were used in the current study. We first determined the expression levels of CAR and integrins (αvβ3 and αvβ5) on the cell surface of glioblastoma cells. To predict the response of human glioblastoma to OBP-301 or OBP-405, the established cell lines U87-MG, U251-MG, D54, and U373-MG and primary MDC-01 cells isolated from glioblastoma tissue were used. The U87-MG, D54 and MDC-01 cells expressed the lowest levels of CAR, whereas the U251-MG cells expressed the highest level of CAR (Figure 1a). In contrast, αvβ3 and αvβ5 integrins were highly expressed in each of these glioblastoma cells. Cells that expressed low levels of CAR were resistant to OBP-301 infection, whereas OBP-405 effectively decreased viabi-

Correspondence: Dr T Yokoyama, Department of Neurosurgery, The University of Texas MD Anderson Cancer Center, Unit BSRB 1004, 1515 Holcombe Blvd., Houston, TX 77030, USA.
E-mail: tyokoyama@mdanderson.org
[8]These authors contributed equally to this work.
Received 26 January 2008; revised 1 April 2008; accepted 1 April 2008; published online 26 June 2008

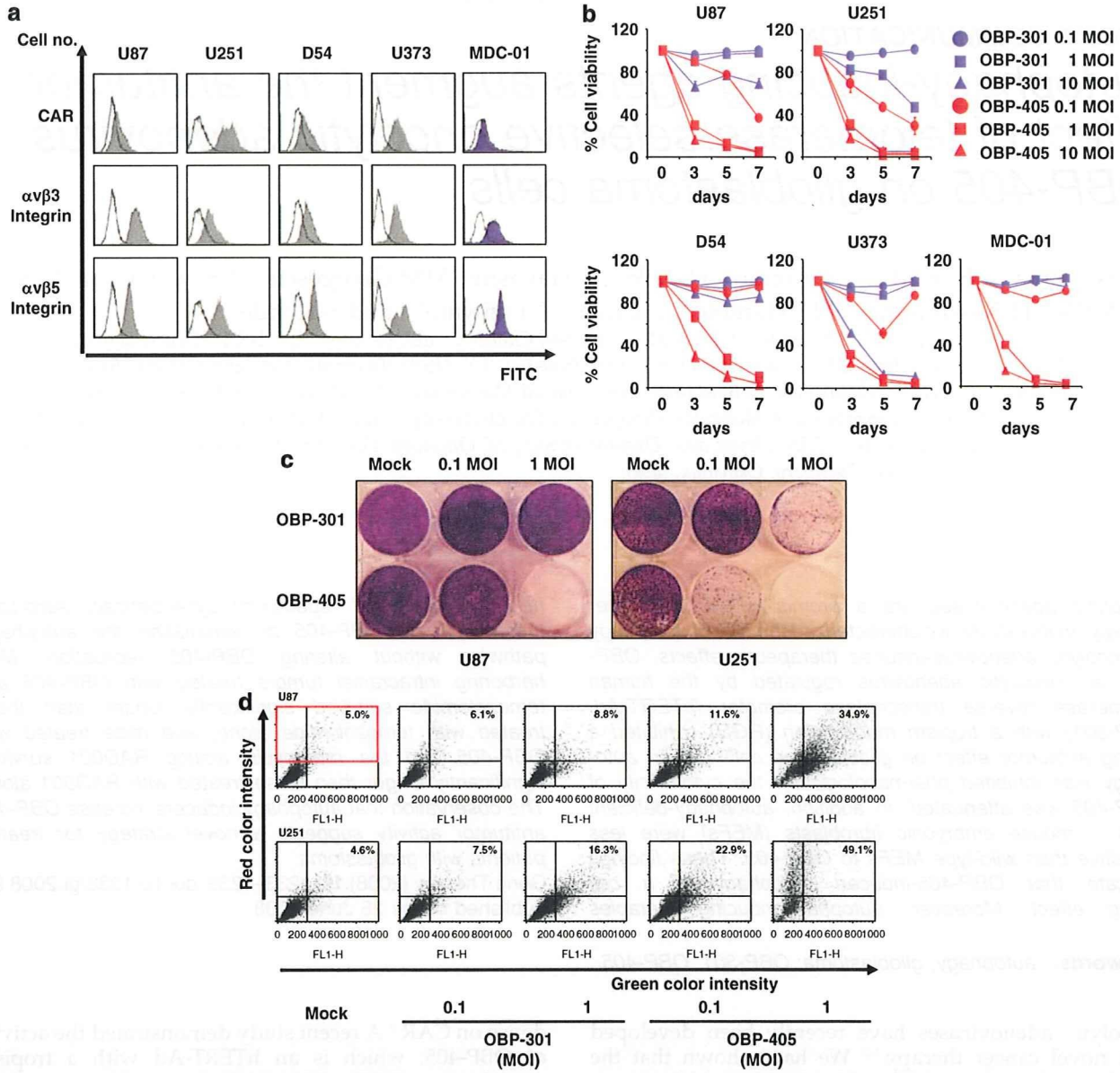

Figure 1 (a) Flow cytometric analysis of CAR and integrin (αvβ3 and αvβ5) expression on glioblastoma cells. Human glioblastoma cell lines U87-MG, U251-MG, D54 and U373-MG were purchased from American Type Culture Collection (Manassas, VA, USA). Primary glioblastoma MDC-01 cells were isolated from surgical specimens of glioblastoma at MD Anderson Cancer Center and were positive for telomerase and glial-fibrillary acidic protein. Cells were incubated with anti-CAR (Upstate Biotechnology, Lake Placid, NY, USA), anti-αvβ3 integrin and anti-á$_v$β5 integrin (Chemicon International, Temecula, CA, USA) monoclonal antibodies and then detected with fluorescein isothiocyanate (FITC)-labeled rabbit anti-mouse IgG secondary antibody (Zymed Laboratories, San Francisco, CA, USA). Open areas (control), isotype-matched normal mouse IgG1 conjugated to FITC. (**b**) Effect of OBP-301 and OBP-405 on the viability of glioblastoma cells. Cells were infected at the indicated MOI values and surviving cells were quantified over 7 days by the use of WST-1 assay (Roche Applied Science, Indianapolis, IN, USA). Results shown are the means ± s.d. of three independent experiments. (c) Oncolytic effect of OBP-301 and OBP-405 on glioblastoma cells. Low-CAR expressing (U87-MG) and high-CAR expressing (U251-MG) cells were stained with 0.5% crystal violet (Sigma-Aldrich, St Louis, MO, USA) 5 days after infection. (**d**) Development of acidic vesicular organelles (AVOs) in U87-MG and U251-MG cells infected with OBP-301 or OBP-405 at an MOI of 0.1 or 1.0 for 72 h. Mock- or virus-infected cells were stained with 1.0 μg ml^{-1} acridine orange (Polysciences, Warrington, PA, USA) for 15 min at room temperature and analyzed using a flow cytometer (FACScan; Becton Dickinson, San Jose, CA, USA). In acridine orange-stained cells, the cytoplasm and nucleus fluorescence bright green and dim red, whereas acidic compartments fluorescence bright red.[10,11] The intensity of the red fluorescence is proportional to the degree of acidity and volume of AVOs. Top of grid was considered as AVOs. CAR, coxsackievirus and adenovirus receptor; IgG, immunoglobulin G; MOI, multiplicity of infection.

lity of glioblastoma cells (Figure 1b). In addition, OBP-405 killed the cells more efficiently than did OBP-301, and neither OBP-301 nor OBP-405 induced apoptosis (Figure 1c) (Supplementary Figures 1a–c).

Nonapoptotic autophagy is characterized by the development of acidic vesicular organelles (AVOs).[10] Compared with mock infection, both OBP-301 and OBP-405 increased the percentage of AVO-positive cells in a multiplicity of infection (MOI)-dependent manner (Figure 1d). As expected, OBP-405 induced the development of AVOs more efficiently than did OBP-301.

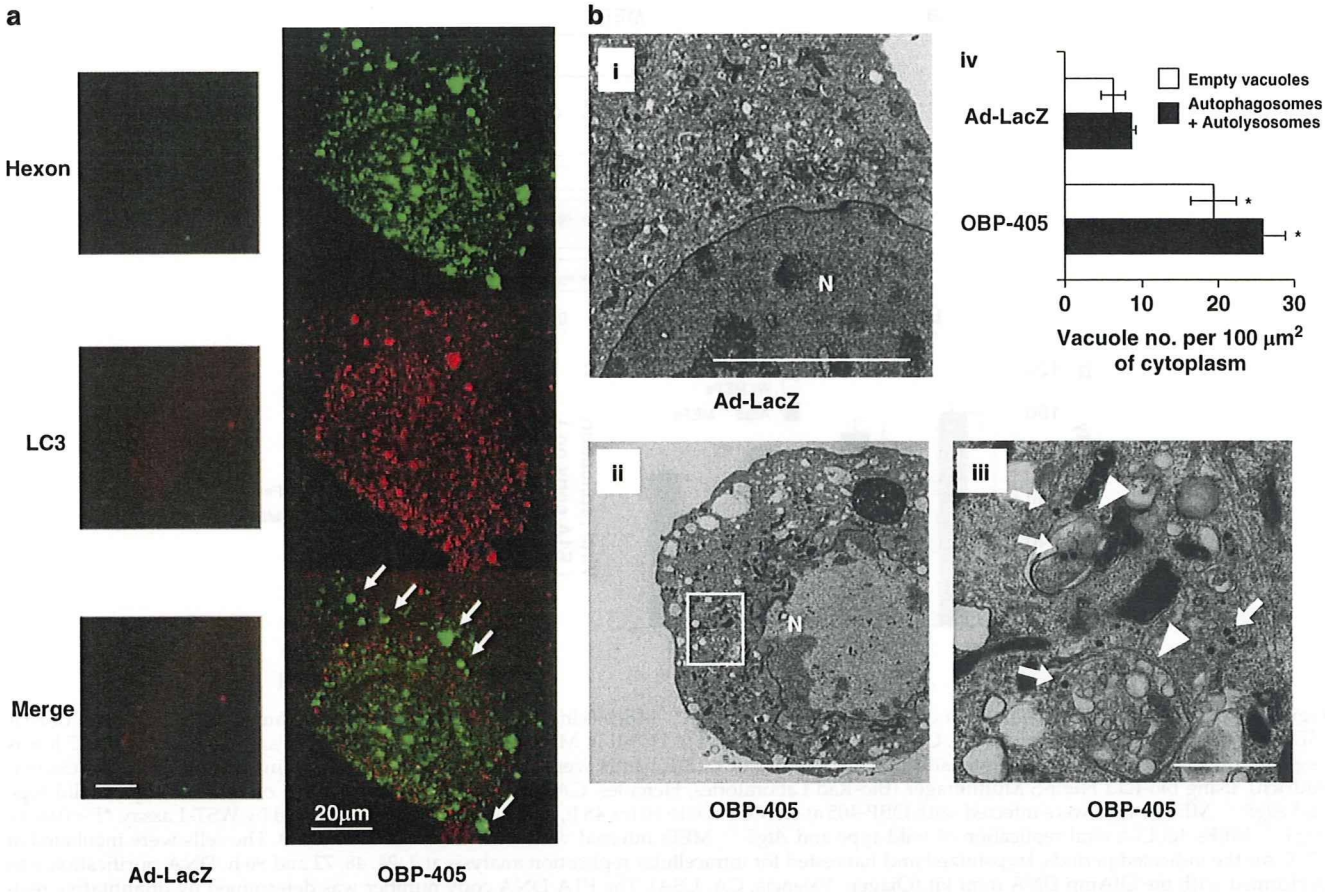

Figure 2 (**a**) Localization of the adenoviral protein hexon and autophagic LC3B protein in glioblastoma cells infected with Ad-LacZ or OBP-405 at an MOI of 0.5. After infection for 72 h, U87-MG cells were processed for fluorescent immunocytostaining with anti-LC3B (1:5000 dilution) and antiadenovirus 1, 2, 5 and 6 hexon (Chemicon International) antibodies. Anti-LC3B antibody was generated as described previously.[14,15] The slides were monitored using inverted microscope (ECRIPSE TE2000-U; Nikon, Melville, NY, USA) and the data were deconvolved and analyzed using AutoQuant's AutoDeBlur software (MediaCybernetics, Bethesda, MD, USA). The arrow shows the colocalization of LC3B and hexon. (**b**) Electron photomicrographs showing the ultrastructure, including the nucleus (N) of glioblastoma cells treated with nonreplicating adenovirus carrying the Ad-LacZ or OBP-405 at an MOI of 0.5 for 72 h. (**i**) Ad-LacZ-infected U87-MG cells; few autophagic vacuoles were observed, scale bar = 10 μm. (**ii**) OBP-405-infected U87-MG cells, scale bar = 10 μm. (**iii**) A magnified view of the area boxed in (ii), scale bar = 1 μm. The arrow indicates viral particles and the arrowhead indicates an autophagosome that includes residual material and virus particles in the cytoplasm. (**iv**) Autophagosomes and autolysosomes were quantified, as described previously.[16,17] $^*P < 0.05$ vs Ad-LacZ. MOI, multiplicity of infection.

The green fluorescent protein (GFP)-tagged expression vector of LC3 is a useful tool with which to detect autophagy.[12] On fluorescence microscopy, GFP-LC3-transfected U87-MG cells showed the diffuse distribution of GFP-LC3 with mock infection, whereas infection with OBP-405 at an MOI of 1.0 resulted in a punctate pattern of GFP–LC3 (Supplementary Figure 2a). This pattern represents autophagic vacuoles and indicated that OBP-405 induced autophagy. With both OBP-301 and OBP-405, the percentage of GFP–LC3 dots increased in an MOI-dependent manner; this increase was considerably higher with OBP-405 than with OBP-301.

The LC3 protein exists in two cellular forms, LC3-I and LC3-II. LC3-I is converted to LC3-II by conjugation to phosphatidylethanolamine, and the amount of LC3-II is closely correlated with the number of autophagosomes.[13] In both U87-MG and U251-MG cells, the amount of LC3-II was increased by infection with OBP-301 or OBP-405 in an MOI-dependent manner and by OBP-405 in a time-dependent manner (Supplementary Figure 2b). These results indicated that OBP-405 caused more autophagy in glioblastoma cells than OBP-301 did.

To analyze the association between adenoviral infection and autophagy, we determined the localization of OBP-405 and autophagic vacuoles. The adenoviral hexon was detected in the cytoplasm 6 h after infection, but at that point, autophagic vacuoles positive for the isoform B of human LC3 (LC3B) were not observed (Supplementary Figure 3), indicating that autophagy was not initiated. Twenty-four hours after infection, hexon was detected in the cytoplasm and nucleus and LC3B-positive autophagic vacuoles were observed. At 48 h, the cell and nucleus had become larger. At 72 h after infection, the majority of the autophagic vacuoles were colocalized with hexon-positive adenoviruses (Figure 2a). In addition, we analyzed the ultrastructure of infected U87-MG cells. U87-MG cells infected with control nonreplicating adenovirus (Ad-LacZ) exhibited few autophagic features, whereas autophagic vacuoles, autolysosomes and empty vacuoles were observed after infection with OBP-405. Most OBP-405-infected cells

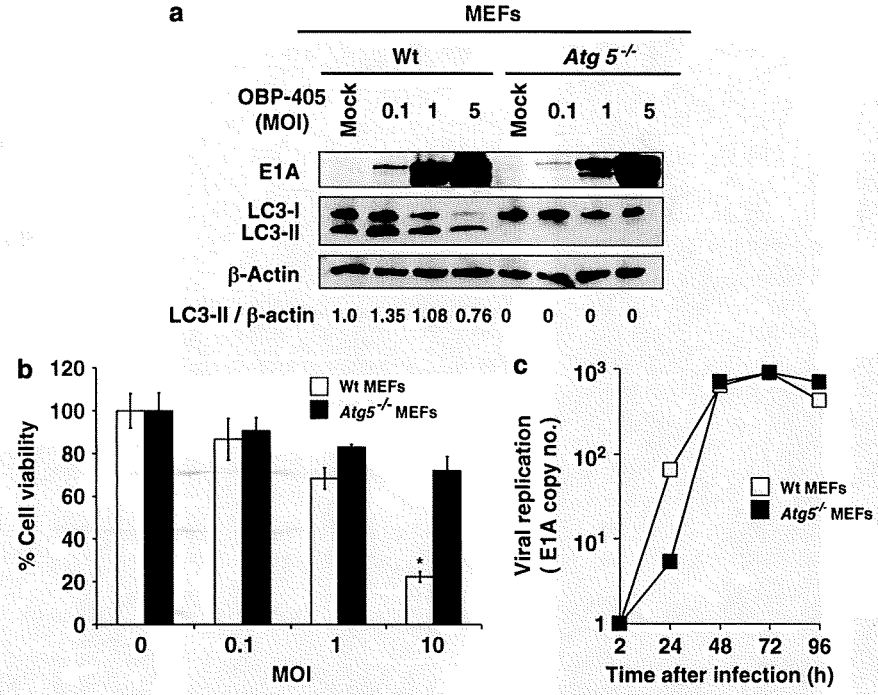

Figure 3 (a) Effect of OBP-405 infection on the wild-type and *Atg5*$^{-/-}$ MEFs (kindly provided by Dr N Mizushima). The expression of E1A (BD Biosciences Pharmingen, San Diego, CA, USA) and an amount of LC3-II in MEFs infected with OBP-405 at an MOI of 0–5.0 for 72 h was assessed by western blotting. The intensities of the amount of LC3-II bands were normalized by the bands' intensities of β-actin (Sigma-Aldrich), using Bio-Rad Fluor-S Multiimager (Bio-Rad Laboratories, Hercules, CA, USA). (**b**) Effect of OBP-405 on the viability of wild-type and *Atg5*$^{-/-}$ MEFs. MEFs were infected with OBP-405 at an MOI of 0 to 10 for 48 h, and cell viability was assessed by WST-1 assay. *$P<0.01$ vs *Atg5*$^{-/-}$ MEFs. (**c**) E1A viral replication of wild-type and *Atg5*$^{-/-}$ MEFs infected with OBP-405 at an MOI of 1.0. The cells were incubated at 37 °C for the indicated periods, trypsinized and harvested for intracellular replication analysis at 2, 24, 48, 72 and 96 h. DNA purification was performed with the QIAmp DNA mini kit (Qiagen, Valencia, CA, USA). The E1A DNA copy number was determined by quantitative real-time PCR, using a Power SYBR Green PCR Master Mix (Applied Biosystems, Foster, CA, USA) and 7500 real-time PCR systems (Applied Biosystems), as described previously.[9] The amount of viral E1A copy number is defined as the fold increase for each sample relative to that at 2 h. MEFs, mouse embryonic fibroblasts; MOI, multiplicity of infection

exhibited viral particles in the nucleus and cytoplasm, but they exhibited neither the chromatin condensation nor the DNA fragmentation that is the characteristic of apoptosis (Figure 2b). Interestingly, viral particles were observed inside autophagic vacuoles. These results suggested that OBP-405 infection initiated the autophagic process and that the autophagic vacuoles sequestered replicating OBP-405.

To assess the role of autophagy in OBP-405 infection, we inhibited the OBP-405-induced autophagy pharmacologically by using 3-methyladenine (3-MA);[18] the decreased viability of these cells was significantly reversed ($P<0.01$) (Supplementary Figures 4a and b). However, the inhibition of autophagy did not affect the increase in E1A copy number of OBP-405 (Supplementary Figure 4c). To exclude the possibility that the effects of 3-MA are independent of inhibition of autophagy, we inhibited autophagy specifically by using small interfering RNA (siRNA) directed against *autophagy-related gene 5* (*Atg5*), which is essential for autophagosome formation. Transfection with *Atg5* siRNA effectively inhibited OBP-405-induced autophagy and recovered the OBP-405-inhibited viability of U87-MG and U251-MG cells (Supplementary Figure 5a–c). Together, the results indicated that OBP-405 induced cell death through autophagy.

In addition, *Atg5*$^{-/-}$ mouse embryonic fibroblasts (MEFs) were significantly more resistant to OBP-405-induced death than the wild-type MEFs ($P<0.01$) (Figures 3a and b). This observation supported our results with 3-MA and *Atg5* siRNA. Similar to 3-MA, viral replication of OBP-405 did not differ significantly between the wild-type and *Atg5*$^{-/-}$ MEFs (Figure 3c).

The above observations prompted us to hypothesize that the antitumor effect of OBP-405 would be augmented by the combinatorial therapy with other autophagy-inducing agents. To test our hypothesis, we combined OBP-405 with rapamycin, an inhibitor of the mammalian target of rapamycin and the DNA-alkylating agent temozolomide (TMZ), both of which efficiently induce autophagy.[19,20] Rapamycin and TMZ not only enhanced OBP-405-induced autophagy *in vitro* but also synergized with OBP-405 to induce the death of glioblastoma cells (Figures 4a and b; Supplementary Figure 6). In contrast, TMZ or rapamycin did not alter viral replication (Figure 4c). Thus OBP-405 synergizes with autophagy-inducing agents to increase cell death *in vitro*.

To determine whether the *in vitro* effect of OBP-405 with TMZ or rapamycin translates to greater activity *in vivo*, we established intracranial tumors in nude mice. Compared with mice treated with Ad-LacZ, mice treated with OBP-405 lived significantly longer (mean survival = 27.5 vs 34.0 days; difference (95% confidence interval) = 6.0 (3.0–9.1) days; $P=0.0008$) (Figure 5a). Mice treated with TMZ also survived significantly longer (mean survival = 27.5 vs 37.0 days; difference = 10

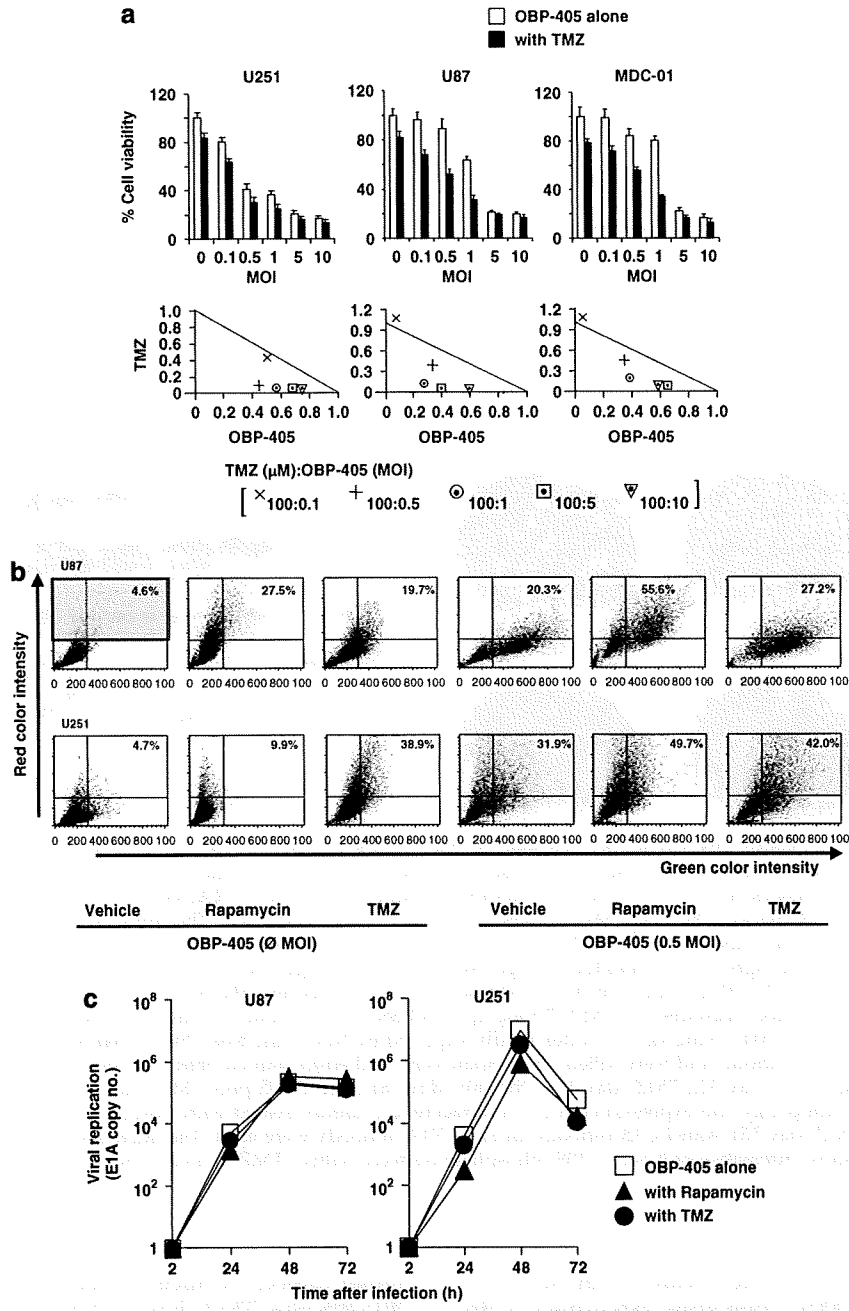

Figure 4 (a) Combined effects of OBP-405 with TMZ on glioblastoma cells. U251-MG, U87-MG and MDC-01 cells were infected with OBP-405 at an MOI of 0 to 10 in the presence of 100 μM TMZ (purchased from a pharmacy in The University of Texas MD Anderson Cancer Center) for 72 h for the WST-1 assay. The combined effect of OBP-405 with TMZ was analyzed with the combination index (CI)-isobologram using CalcuSyn software (Biosoft, Ferguson, MO, USA), as described previously.[19] In the isobologram, a plot on the diagonal line indicates that the combination is simply additive. A plot to the left under the line indicates that the combination is synergistic, whereas a plot to the right above the line indicates that it is antagonistic. Each plot represents values generated in at least three independent experiments for the simultaneous treatment of cells. (**b**) Development of acidic vesicular organelles (AVOs) in U87-MG and U251-MG cells infected with OBP-405 at an MOI of 0.5 in the presence of 1 nM rapamycin (Sigma-Aldrich) or 100 μM TMZ were stained with 1.0 μg ml^{-1} acridine orange as described previously.[10,11] Top of grid was considered as AVOs. (**c**) E1A viral replication of U87-MG and U251-MG cells infected with OBP-405 at an MOI of 0.5 alone or with 1 nM rapamycin or 100 μM TMZ over 72 h as described previously.[9] MOI, multiplicity of infection; TMZ, temozolomide.

(7.0–12) days; $P<0.001$), but RAD001-treated mice did not (mean survival = 27.5 vs 30.5 days; difference = 4 (−1 to 9) days; $P=0.14$). Strikingly, mice treated with OBP-405 and TMZ survived significantly longer than those treated with TMZ alone (mean = 53.0 vs 37.0 days; difference = 15.1 (7.2–23.1) days; $P=0.0015$), and mice treated with OBP-405 and RAD001 survived significantly longer than those treated with RAD001 alone (mean = 38.0 vs 30.5 days; difference = 9.3 (1.7–16.8) days, $P=0.021$). Finally, compared with results using OBP-405 alone, the survival time of mice was significantly prolonged by combination with TMZ (difference = 19 (11–26) days, $P=0.0001$) or RAD001 (difference = 7 (1–13) days, $P=0.025$).

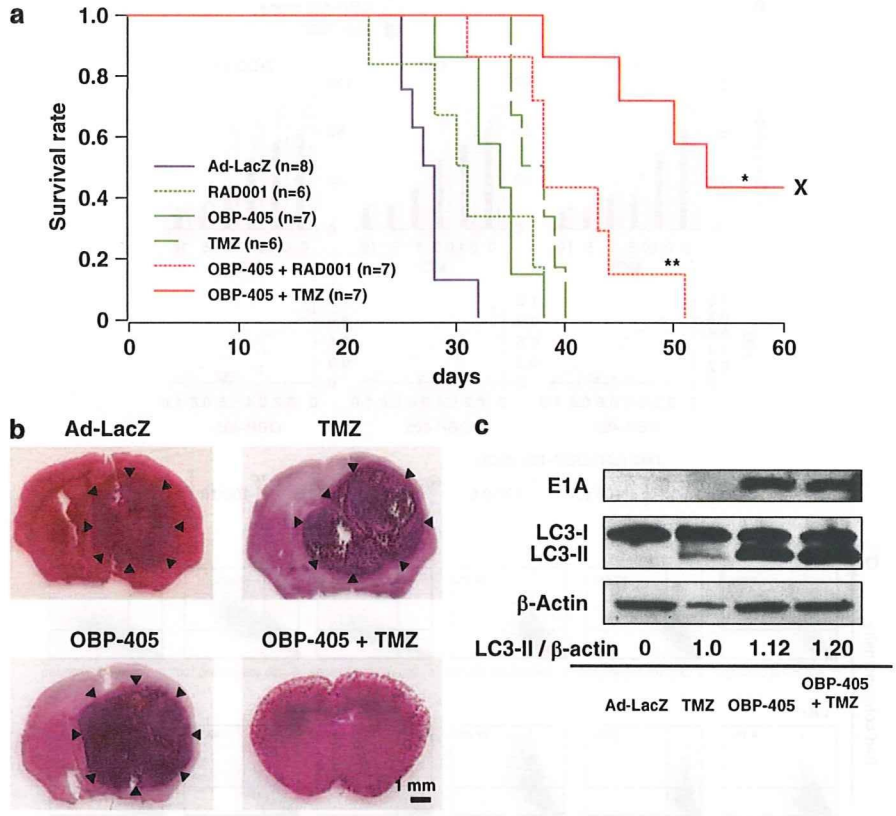

Figure 5 (a) Curves showing overall survival of mice bearing U87-MG intracranial tumors treated with Ad-LacZ, RAD001, TMZ, OBP-405, OBP-405 plus RAD001 or OBP-405 plus TMZ. The Kaplan–Meier method and pooled-variance two-tailed t-test were used to assess the statistical significance of differences in survival time; $^{*}P = 0.0015$ vs TMZ; $^{**}P = 0.021$ vs RAD001; 8- to 12-week-old female nude mice (Department of Experimental Radiation Oncology, MD Anderson Cancer Center) were used. The intracranial tumor model using U87-MG cells (5×10^5) was established as described previously.[3] Three days after the inoculation of U87-MG cells (day 0), the treatments were initiated as follows. On days 3, 5 and 7, through a 10 μl Hamilton syringe fitted with a 26-gauge needle connected to a microinfusion pump, Ad-LacZ (2.2×10^9 pfu ml^{-1}) or OBP-405 (2.2×10^9 pfu ml^{-1}) in 10 μl of sterile PBS was infused into the tumors through the screw guide at a depth of 3.5 mm from the skull. Two hundred microliters of TMZ (7.5 mg kg^{-1} in PBS with 5% dimethyl sulfoxide) was injected intraperitoneally five times a week for 2 weeks, and RAD001 (5 mg kg^{-1} in water, kindly supplied by Norvartis, Basel, Switzerland) was administered orally every day until the animals became moribund and were killed. (**b**) Hematoxylin and eosin-stained brain tissues of mice bearing intracranial U87-MG tumors treated with Ad-LacZ (day 32), TMZ (day 40), OBP-405 (day 38) or OBP-405 plus TMZ (day 60). Scale bar = 1 mm. (**c**) Western blots showing induction of autophagy and expression of E1A in intracerebral tumors treated with Ad-LacZ (day 28), TMZ (day 39), OBP-405 (day 35) or OBP-405 plus TMZ (day 53). Anti-LC3B antibody and anti-E1A antibody were used. The intensities of the amount of LC3-II bands were normalized by the bands' intensities of β-actin. PBS, phosphate-buffered saline; TMZ, temozolomide.

The intracranial tumors of mice treated with Ad-LacZ, OBP-405, TMZ or RAD001 alone grew extensively, with midlines shifted laterally. Strikingly, tumors were undetectable in brain tissue harvested from three mice treated with OBP-405 plus TMZ that survived 60 days after inoculation (Figure 5b). Hexon was detected in the intracranial tumor treated with OBP-405 plus TMZ (day 45) but not in the tumor treated with Ad-LacZ (day 28) (Supplementary Figure 7). This finding was supported by western blotting results showing detectable E1A protein expression in intracranial tumors treated with OBP-405 alone or with TMZ (Figure 5c). These results indicated that OBP-405 replicated and spread through the intracranial tumors but not through the normal brain tissues and supported the contention that the effect of OBP-405 is specific to tumors, likely due to the hTERT promoter activity. Then, we determined whether the induction of autophagy is detected under *in vivo* settings using an anti-LC3B-specific antibody. As shown in Figure 5c, the amount of LC3-II was higher in intracranial tumors of mice treated with TMZ, OBP-405 and OBP-405 plus TMZ than in Ad-LacZ-treated mice. These results indicated that autophagy was induced in intracranial tumors of mice as well as *in vitro* and that the extent of autophagy was enhanced by the combination treatment. However, intracranial tumors established from noninvasive glioblastoma cell lines may limit the clinical relevance of studies assessing the efficacy of novel therapies.[21] Therefore, we will further assess whether the treatment with OBP-405 plus TMZ or RAD001 prolong the survival of the mice carrying invasive intracranial tumors.[21]

In conclusion, we found that the fiber-modified hTERT-Ad OBP-405 has a marked antitumor effect on glioblastoma cells regardless of the cellular expression level of CAR. Moreover, autophagy-inducing agents (TMZ and rapamycin) increase the *in vitro* and *in vivo* antitumor activity of OBP-405 through the enhancement of autophagic pathway. A recent clinical study showed that TMZ had antitumor activity both as a single agent

and as adjuvant chemotherapy for patients with malignant gliomas, although its efficacy was modest.[22] Our study results might indicate a new way to treat glioblastomas with a combination of autophagy-inducing agents.

Acknowledgements

We thank Dr Noboru Mizushima for the GFP-LC3 expression vector and the wild-type and *Atg5−/−* MEFs. We also thank E Faith Hollingsworth for technical support and Elizabeth L Hess for editing the manuscript. This work was supported in part by Grant CA-088936 from the National Cancer Institute (to S Kondo), by a generous donation from the Anthony D Bullock III Foundation (to Y Kondo, R Sawaya and S Kondo) and the Institutional Core Grant CA-16672 High Resolution Electron Microscopy Facility, MD Anderson Cancer Center.

Grant support: This study was supported in part by National Cancer Institute Grants CA088936 and CA108558, a start-up fund from The University of Texas MD Anderson Cancer Center (SK), a generous donation from the Anthony D Bullock III Foundation (YK, RS and SK) and the cancer center support grant (CCSG)/shared resources of MD Anderson Cancer Center.

References

1 Mathis JM, Stoff-Khalili MA, Curiel DT. Oncolytic adenoviruses-selective retargeting to tumor cells. *Oncogene* 2005; **24**: 7775–7791.
2 Ko D, Hawkins L, Yu DC. Development of transcriptionally regulated oncolytic adenoviruses. *Oncogene* 2005; **24**: 7763–7774.
3 Ito H, Aoki H, Kühnel F, Kondo Y, Kubicka S, Wirth T *et al.* Autophagic cell death of malignant glioma cells induced by a conditionally replicating adenovirus. *J Natl Cancer Inst* 2006; **98**: 625–636.
4 Ogier-Denis E, Codogno P. Autophagy: a barrier or an adaptive response to cancer. *Biochim Biophys Acta* 2003; **1603**: 113–128.
5 Gozuacik D, Kimchi A. Autophagy as a cell death and tumor suppressor mechanism. *Oncogene* 2004; **23**: 2891–2906.
6 Kondo Y, Kanzawa T, Sawaya R, Kondo S. The role of autophagy in cancer development and response to therapy. *Nat Rev Cancer* 2005; **5**: 726–734.
7 Wickham TJ, Mathias P, Cheresh DA, Nemerow GR. Integrins $\alpha_v\beta_3$ and $\alpha_v\beta_5$ promote adenovirus internalization but not virus attachment. *Cell* 1993; **73**: 309–319.
8 Hedley SJ, Chen J, Mountz JD, Li J, Curiel DT, Korokhov N *et al.* Targeted and shielded adenovectors for cancer therapy. *Cancer Immunol Immunother* 2006; **55**: 1412–1419.
9 Taki M, Kagawa S, Nishizaki M, Mizuguchi H, Hayakawa T, Kyo S *et al.* Enhanced oncolysis by a tropism-modified telomerase-specific replication-selective adenoviral agent OBP-405 ('Telomelysin-RGD'). *Oncogene* 2005; **24**: 3130–3140.
10 Klionsky DJ, Cuervo AM, Seglen PO. Methods for monitoring autophagy from yeast to human. *Autophagy* 2007; **3**: 181–206.
11 Paglin S, Hollister T, Delohery T, Hackett N, McMahill M, Sphicas E *et al.* A novel response of cancer cells to radiation involves autophagy and formation of acidic vesicles. *Cancer Res* 2001; **61**: 439–444.
12 Mizushima N. Methods for monitoring autophagy. *Int J Biochem Cell Biol* 2004; **36**: 2491–2502.
13 Mizushima N, Yoshimori T. How to interpret LC3 immunoblotting. *Autophagy* 2007; **3**: 542–545.
14 Aoki H, Takada Y, Kondo S, Sawaya R, Aggarwal BB, Kondo Y. Evidence that curcumin suppresses the growth of malignant gliomas *in vitro* and *in vivo* through induction of autophagy: role of Akt and extracellular signal-regulated kinase signaling pathways. *Mol Pharmacol* 2007; **72**: 29–39.
15 Aoki H, Kondo Y, Aldape K, Yamamoto A, Iwado E, Yokoyama T *et al.* Monitoring Autophagy in Glioblastoma with Antibody against Isoform B of Human Microtubule-Associated Protein 1 Light Chain 3. *Autophagy* 2008; **4**: 467–475.
16 Klionsky DJ, Abeliovich H, Agostinis P, Agrawal DK, Aliev G, Askew DS *et al.* Guidelines for the use and interpretation of assays for monitoring autophagy in higher eukaryotes. *Autophagy* 2008; **4**: 151–175.
17 Tanida I, Minematsu-Ikeguchi N, Ueno T, Kominami E. Lysosomal turnover, but not a cellular level, of endogenous LC3 is a marker for autophagy. *Autophagy* 2005; **1**: 84–91.
18 Shintani T, Klionsky DJ. Autophagy in health and disease: a double-edged sword. *Science* 2004; **306**: 990–995.
19 Takeuchi H, Kondo Y, Fujiwara K, Kanzawa T, Aoki H, Mills GB *et al.* Synergistic augmentation of rapamycin-induced autophagy in malignant glioma cells by phosphatidylinositol 3-kinase/protein kinase B inhibitors. *Cancer Res* 2005; **65**: 3336–3346.
20 Kanzawa T, Germano IM, Komata T, Ito H, Kondo Y, Kondo S. Role of autophagy in temozolomide-induced cytotoxicity for malignant glioma cells. *Cell Death Differ* 2004; **11**: 448–457.
21 Giannini C, Sarkaria JN, Saito A, Uhm JH, Galanis E, Carlson BL *et al.* Patient tumor EGFR and PDGFRA gene amplifications retained in an invasive intracranial xenograft model of glioblastoma multiforme. *Neuro Oncol* 2005; **7**: 164–176.
22 Stupp R, Mason WP, van den Bent MJ, Weller M, Fisher B, Taphoorn MJ *et al.* Radiotherapy plus concomitant and adjuvant temozolomide for glioblastoma. *N Engl J Med* 2005; **352**: 987–996.

Supplementary Information accompanies the paper on Gene Therapy website (http://www.nature.com/gt)

Telomerase-Specific Virotheranostics for Human Head and Neck Cancer

Yuji Kurihara,[1] Yuichi Watanabe,[2,3] Hideki Onimatsu,[2] Toru Kojima,[4] Tatsuo Shirota,[1] Masashi Hatori,[1] Dong Liu,[5] Satoru Kyo,[6] Hiroyuki Mizuguchi,[7] Yasuo Urata,[2] Satoru Shintani,[1] and Toshiyoshi Fujiwara[3,4]

Abstract

Purpose: Long-term outcomes of patients with squamous cell carcinoma of the head and neck (SCCHN) remain unsatisfactory despite advances in combination of treatment modalities. SCCHN is characterized by locoregional spread and it is clinically accessible, making it an attractive target for intratumoral biological therapies.

Experimental Design: OBP-301 is a type 5 adenovirus that contains the replication cassette in which the human telomerase reverse transcriptase promoter drives expression of the *E1* genes. OBP-401 contained the replication cassette and the green fluorescent protein (*GFP*) gene. The antitumor effects of OBP-301 were evaluated *in vitro* by the sodium 30-[1-(phenylaminocarbonyl)-3,4-tetrazolium]-bis(4-methoxy-6-nitro)benzene sulfonic acid hydrate assay and *in vivo* in an orthotopic xenograft model. Virus spread into the lymphatics was also orthotopically assessed by using OBP-401.

Results: Intratumoral injection of OBP-301 resulted in the shrinkage of human SCCHN tumors orthotopically implanted into the tongues of BALB/c *nu/nu* mice and significantly recovered weight loss by enabling oral ingestion. The levels of GFP expression following *ex vivo* infection of OBP-401 may be of value as a positive predictive marker for the outcome of telomerase-specific virotherapy. Moreover, whole-body fluorescent imaging revealed that intratumorally injected OBP-401 could visualize the metastatic lymph nodes, indicating the ability of the virus to traffic to the regional lymphatic area and to selectively replicate in neoplastic lesions, resulting in GFP expression and cell death in metastatic lymph nodes.

Conclusions: These results illustrate the potential of telomerase-specific oncolytic viruses for a novel therapeutic and diagnostic approach, termed theranostics, for human SCCHN.

Cancer remains a leading cause of death worldwide despite improvements in diagnostic techniques and clinical management (1, 2). An estimated 500,000 patients worldwide are diagnosed with squamous cell carcinoma of the head and neck (SCCHN) annually. This aggressive epithelial malignancy is associated with a high mortality rate and severe morbidity among the long-term survivors (3). Current treatment strategies for advanced SCCHN include surgical resection, radiation, and cytotoxic chemotherapy. Although a combination of these modalities can improve survival, most patients eventually experience disease progression that leads to death; disease progression is often the result of intrinsic or acquired resistance to treatment (4, 5). A lack of specificity for tumor cells is the primary limitation of radiotherapy and chemotherapy. To improve the therapeutic index, there is a need for anticancer agents that selectively target only tumor cells and spare normal cells.

Replication-selective tumor-specific viruses present a novel approach for cancer treatment (6, 7). We reported previously that telomerase-specific replication-competent adenovirus (OBP-301, Telomelysin), in which the human telomerase reverse transcriptase (hTERT) promoter element drives the expression of *E1A* and *E1B* genes linked with an IRES, induced selective E1 expression, and efficiently killed human cancer cells but not normal cells (8–10). We also found that intratumoral injection of telomerase-specific replication-selective adenovirus expressing the green fluorescent protein (*GFP*) gene (OBP-401, TelomeScan) causes viral spread into the regional lymphatic area with subsequent selective replication in

Authors' Affiliations: [1]Department of Oral and Maxillofacial Surgery, School of Dentistry, Showa University and [2]Oncolys BioPharma, Inc., Tokyo, Japan; [3]Center for Gene and Cell Therapy, Okayama University Hospital and [4]Division of Surgical Oncology, Department of Surgery, Okayama University Graduate School of Medicine, Dentistry and Pharmaceutical Sciences, Okayama, Japan; [5]Research Center of Lung Cancer, Shanghai Pulmonary Hospital, Shanghai, China; [6]Department of Obstetrics and Gynecology, Kanazawa University School of Medicine, Kanazawa, Japan; and [7]Department of Biochemistry and Molecular Biology, Graduate School of Pharmaceutical Sciences, Osaka University, Osaka, Japan

Received 10/22/08; revised 12/17/08; accepted 12/31/08; published OnlineFirst 3/24/09.

Grant support: Grants-in-Aid from the Ministry of Education, Science, and Culture, Japan (T. Fujiwara), and Grants from the Ministry of Health and Welfare, Japan (T. Fujiwara).

The costs of publication of this article were defrayed in part by the payment of page charges. This article must therefore be hereby marked *advertisement* in accordance with 18 U.S.C. Section 1734 solely to indicate this fact.

Note: Supplementary data for this article are available at Clinical Cancer Research Online (http://clincancerres.aacrjournals.org/).

Requests for reprints: Toshiyoshi Fujiwara, Center for Gene and Cell Therapy, Okayama University Hospital, 2-5-1 Shikata-cho, Okayama 700-8558, Japan. Phone: 81-86-235-7997; Fax: 81-86-235-7884; E-mail: toshi_f@md.okayama-u.ac.jp.

doi:10.1158/1078-0432.CCR-08-2690

Translational Relevance

Despite new therapeutic modalities, long-term outcomes of patients with squamous cell carcinoma of the head and neck (SCCHN) remain unsatisfactory. Thus, the development of efficient treatment methods to enable the reduction of tumors in these patients is clearly imperative. Tumor-targeted oncolytic viruses have the potential to selectively infect target tumor cells, multiply, and cause cell death and release of viral particles, leading to the spread of viral-mediated antitumor effects. We developed a telomerase-specific oncolytic adenovirus OBP-301 (Telomelysin) as well as OBP-401 – expressing *GFP* gene (TelomeScan). Our data showed that telomerase-specific oncolytic viruses can be effective to kill human SCCHN cells *in vitro* and *in vivo* as well as to identify the patients who will likely benefit from virotherapy, suggesting that an oncolytic virus-based approach exhibited desirable features of a novel "virotheranostics," the combination of a diagnostic assay with a therapeutic entity for human SCCHN. This is a preclinical study for the future clinical trials.

metastatic lymph nodes in *nu/nu* mice (11). Although up to 25% of patients with SCCHN develop distant metastasis to the lung, liver, or bone, lymph node metastases are more common in SCCHN patients (12); therefore, locoregional disease control with telomerase-specific oncolytic viruses may be a novel therapeutic strategy that is clinically applicable for the treatment of human SCCHN.

In the present study, we explore the therapeutic as well as diagnostic ability of telomerase-specific oncolytic viruses *in vitro* and *in vivo*. To this end, we adopted an orthotopic head and neck cancer xenograft model by inoculating human SCCHN cells into the tongues of *nu/nu* mice; this model resembles human SCCHN in a number of biological properties (13).

Materials and Methods

Cell lines and cell culture. The human oral squamous carcinoma cell lines SAS-L, SCC-4, SCC-9, HSC-2, HSC-3, and HSC-4 were maintained *in vitro* as monolayers in DMEM supplemented with 10% heat-inactivated fetal bovine serum, 100 units/mL penicillin, and 100 mg/mL streptomycin (complete medium). The human non–small-cell lung cancer cell line H460 and the human esophageal cancer cell line TE8 were routinely propagated in monolayer culture in RPMI 1640 supplemented with 10% fetal bovine serum. The normal human lung diploid fibroblast cell line WI38 (JCRB0518) was obtained from the Health Science Research Resources Bank (Osaka, Japan) and grown in Eagle's MEM with 10% fetal bovine serum. The normal human lung fibroblast NHLF (TaKaRa Biomedicals) and the normal human embryonic lung fibroblast MRC-5 (RIKEN BioResource Center) were cultured according to the vendors' specifications.

Adenoviruses. The recombinant replication-selective, tumor-specific adenovirus vector OBP-301 (Telomelysin), in which the hTERT promoter element drives the expression of *E1A* and *E1B* genes linked with an IRES, was previously constructed and characterized (8–10). OBP-401 is a telomerase-specific replication-competent adenovirus variant with the replication cassette, and *GFP* gene under the control of the cytomegalovirus promoter was inserted into the E3 region for monitoring viral replication (11, 14). The viruses were purified by ultracentrifugation in cesium chloride step gradients, their titers were determined by a plaque-forming assay using 293 cells, and they were stored at -80°C.

Cell viability assay. An sodium 30-[1-(phenylaminocarbonyl)-3,4-tetrazolium]-bis(4-methoxy-6-nitro)benzene sulfonic acid hydrate (XTT) assay was done to assess the viability of tumor cells. Human SCCHN cells (1,000 per well) were seeded onto 96-well plates 18 to 20 h before viral infection. Cells were then infected with OBP-301 at a multiplicity of infection (MOI) of 1, 10, 50, and 100 plaque-forming units (pfu) per cell. Cell viability was determined at the indicated time points by using a Cell Proliferation Kit II (Roche Molecular Biochemicals) according to the protocol provided by the manufacturer.

Fluorescence microplate reader. Cells were infected with OBP-401 at the indicated MOI values in a 96-well black-bottomed culture plate and further incubated for the indicated time periods. GFP fluorescence was measured by using a fluorescence microplate reader (DS Pharma Biomedical) with excitation/emission at 485 nm/528 nm.

Animal experiments. SAS-L and HSC-3 human oral squamous cell carcinoma cells were harvested and suspended at a concentration of 5×10^6/mL in the medium. To generate an orthotopic head and neck cancer model, 6-wk-old female BALB/c *nu/nu* mice were anesthetized and injected directly with 20 μL of cell suspension at a density of 10^5 cells. The cells were injected into the right lateral border of the tongue with a 27-gauge needle. When the tumor grew to 2 to 3 mm in diameter ~5 to 7 days later, 20 μL of solution containing 1×10^8 pfu of OBP-301, OBP-401, or PBS were injected into the tumor. The perpendicular diameter of each tumor was measured every 3 d, and tumor volume was calculated by using the following formula: tumor volume (mm^3) = $a \times b^2 \times 0.5$, where a is the longest diameter, b is the shortest diameter, and 0.5 is a constant to calculate the volume of an ellipsoid. The body weights of mice were monitored and recorded. The experimental protocol was approved by the Ethics Review Committee for Animal Experimentation of Okayama University.

In vivo *fluorescence imaging.* *In vivo* GFP fluorescence imaging was acquired by illuminating the animal with a Xenon 150-W lamp. The reemitted fluorescence was collected through a long-pass filter on a Hamamatsu C5810 3-chip color charge-coupled device camera (Hamamatsu Photonics Systems). High-resolution image acquisition was accomplished by using an EPSON PC. Images were processed for contrast and brightness with the use of Adobe Photoshop 4.0.1J software (Adobe). A fluorescence stereomicroscope (SZX7; Olympus) was also used to visualize GFP-positive tissues.

Statistical analysis. The statistical significance of the differences in the *in vitro* and *in vivo* antitumor effects of viruses was determined by using the Student's t test (two-tailed). The antitumor effect viruses on orthotopically implanted tumors in nude mice were assessed by plotting survival curves according to the Kaplan-Meier method. P values <0.05 were considered statistically significant.

Results

In vitro ***cytopathic efficacy of OBP-301 on human SCCHN cell lines.*** We examined the cytopathic effect of OBP-301, which is an attenuated adenovirus in which the hTERT promoter element drives expression of *E1A* and *E1B* genes linked with an internal ribosome entry site (IRES; Fig. 1A), on various human SCCHN cell lines by the XTT cell viability assay. OBP-301 infection induced cell death in human SCCHN cells in a dose-dependent manner; the sensitivity, however, varied among different cell lines (Fig. 1B). The ID_{50} values calculated from the dose-response curves confirmed that SAS-L cells could be efficiently killed by OBP-301 at an multiplicity of infection (MOI) of <150 (ID_{50} = 148), whereas HSC-3 cells were less sensitive to OBP-301 (ID_{50} = 500; Fig. 1C).

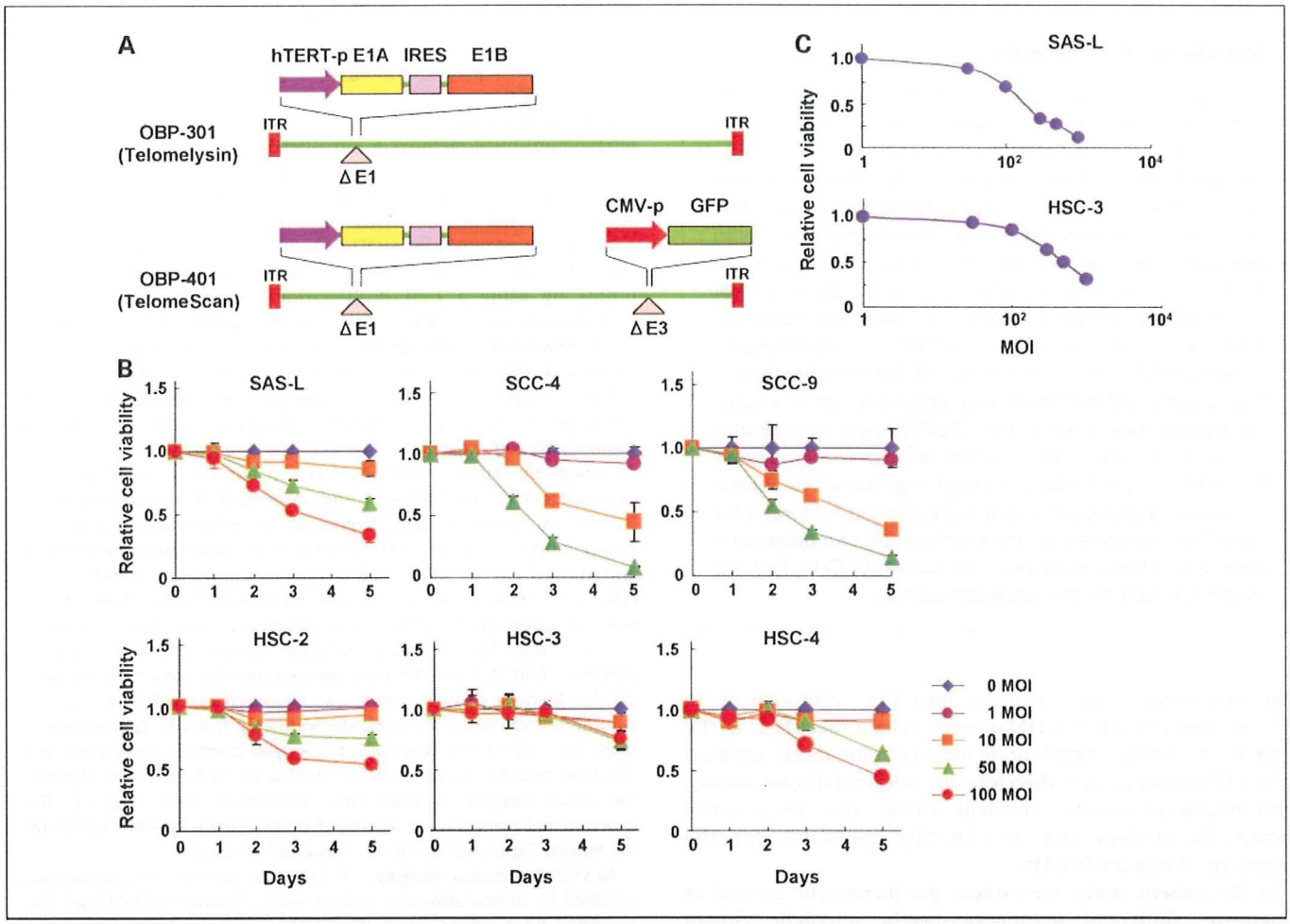

Fig. 1. Schematic DNA structures of telomerase-specific viruses and selective cytopathic effect in human SCCHN cell lines *in vitro*. *A*, OBP-301 is a telomerase-specific replication-competent adenovirus containing the hTERT promoter sequence inserted into the adenovirus genome to drive transcription of the E1A and E1B bicistronic cassette linked by the IRES. OBP-401 is a variant of OBP-301, in which the *GFP* gene is inserted under the cytomegalovirus (*CMV*) promoter into the E3 region for monitoring viral replication. *B*, human SCCHN cell lines were infected with OBP-301 at the indicated MOI values, and surviving cells were quantitated over 5 d by the XTT assay. The cell viability of mock-treated cells on day 0 was considered 1.0, and the relative cell viability was calculated. Points, mean of triplicate experiments; bars, SD. *C*, effects of various concentrations of OBP-301 on SAS-L and HSC-3 cells assessed 5 d after the XTT assay. Results are expressed as the relative cell viability of untreated control cells.

To confirm the specificity of telomerase activity in human SCCHN cells, we next measured the expression of *hTERT* mRNA in a panel of human SCCHN cell lines and normal cell lines by using a real-time reverse transcription-PCR method. Although the levels of expression varied widely, all SCCHN cell lines expressed detectable levels of *hTERT* mRNA, whereas human fibroblast cells such as NHLF and WI38 were negative for *hTERT* expression (Supplementary Fig. S1A). We also examined the expression levels of coxsackievirus and adenovirus receptor on the cell surface of each type of cell by flow cytometric analysis. Apparent amounts of coxsackievirus and adenovirus receptor expression were detected on SAS-L and HSC-3 human SCCHN cells (Supplementary Fig. S1B).

To assess whether viral replication was restricted to tumor cells, we next examined the replication ability of OBP-301 by measuring the relative amounts of E1A DNA. SAS-L human SCCHN cells and MRC-5 human fibroblasts were harvested at indicated time points over 72 h after infection with OBP-301 and subjected to quantitative real-time PCR analysis. The ratios were normalized by dividing the value of cells obtained 2 h after viral infection. OBP-301 replicated 3 to 4 logs within 48 h after infection; the viral replication, however, was attenuated up to 2 logs in normal MRC-5 cells (Supplementary Fig. S2).

The response of tumor cells to DNA-damaging stimuli such as chemotherapeutic drugs and ionizing radiation is predetermined by the functional status of their *p53* gene (15); however, the p53 status of human SCCHN cell lines (wild-type p53 [SAS-L], mutant p53 [SCC-4, HSC-2, HSC-3, HSC-4], and deleted p53 [SCC-9]) is not related to their sensitivity to OBP-301. Indeed, OBP-301 similarly killed parental SAS-L cells and cells stably transfected with the mutant *p53* gene (Supplementary Fig. S3), suggesting that OBP-301 induces cell death in a p53-independent manner.

Selective replication of OBP-401 in human SCCHN cell lines in vitro. OBP-401 is a genetically engineered adenovirus that expresses GFP by inserting the *GFP* gene under the control of the cytomegalovirus promoter at the deleted E3 region of OBP-301 (Fig. 1A). To determine whether OBP-401 replication is associated with selective GFP expression in human SCCHN cells, cells were analyzed and recorded by using a time-lapse fluorescent microscope after OBP-401 infection. Representative images at the indicated time points are shown (Fig. 2A). SAS-L

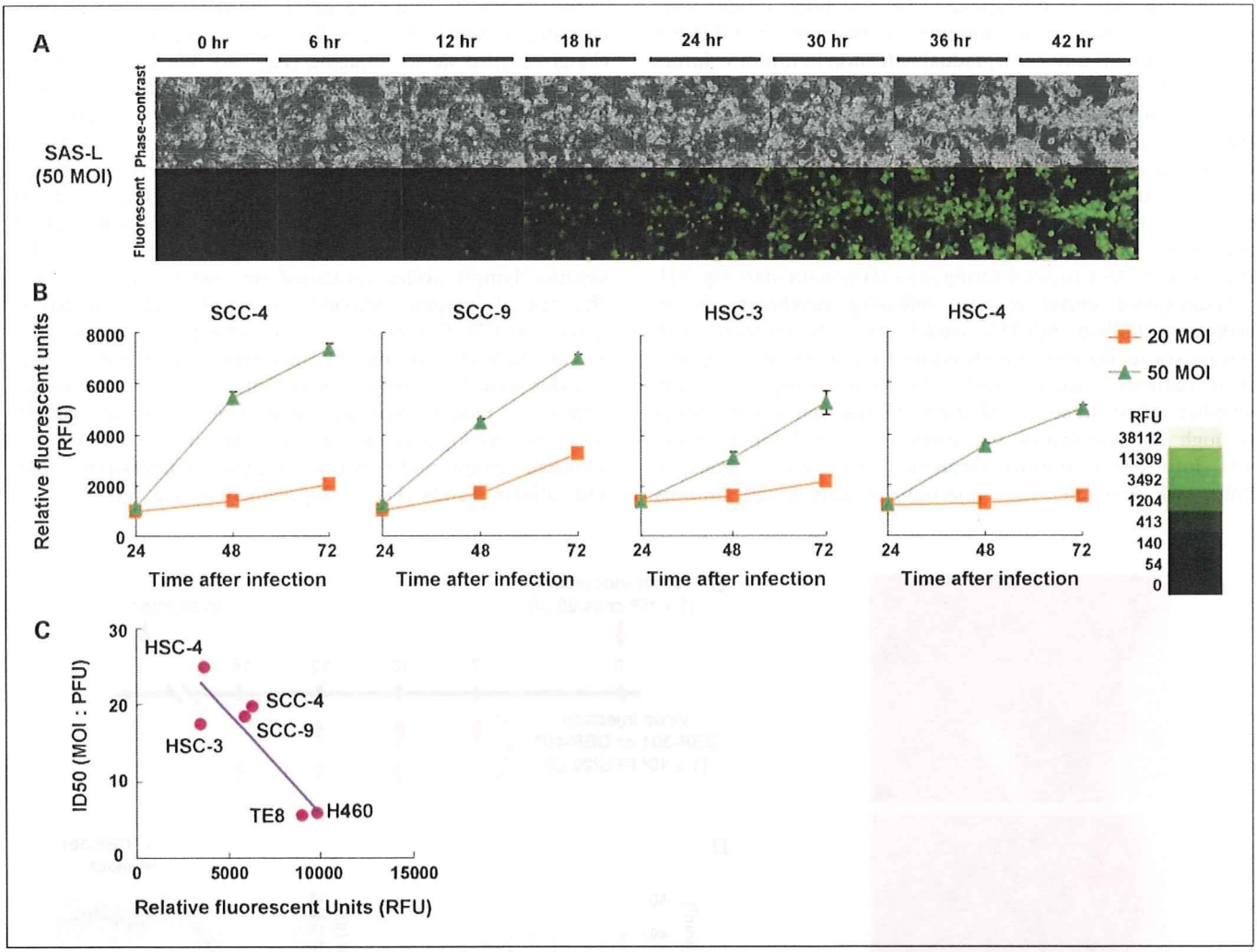

Fig. 2. Selective visualization of human SCCHN cells *in vitro* by OBP-401. *A*, time-lapse images of SAS-L cells were recorded for 42 h after OBP-401 infection at a MOI of 50. Representative images taken at the indicated time points show cell morphology by phase-contrast microscopy (*top*) and GFP expression under fluorescence microscopy (*bottom*). Magnification, ×200. *B*, quantitative assessment of GFP labeling by OBP-401 in human SCCHN cell lines. Cells were infected with OBP-401 at the indicated MOI values, and GFP fluorescence was measured over 72 h by the fluorescence microplate reader. The intensity of green fluorescence was evaluated based on the brightness determinations used as relative fluorescence units (*RFU*). The relative fluorescence unit and time after infection were plotted on the ordinate and abscissa, respectively. A green color calibration bar for the indicated relative fluorescence unit is shown on the right. *C*, relationship between GFP fluorescence after OBP-401 infection and ID_{50} values after OBP-301 infection in human cancer cell lines, including SCCHN cells. Relative GFP fluorescence was measured by the fluorescence microplate reader 72 h after OBP-401 infection at a MOI of 50. The ID_{50} values of OBP-301 on cell viability at 5 d after infection were calculated and expressed as ID_{50} values. The slope represents the inverse correlation between these two factors ($R^2 = 0.7839$).

human SCCHN cells expressed bright GFP fluorescence as early as 12 h after OBP-401 infection at a MOI of 50. The fluorescence intensity gradually increased in a dose-dependent manner, followed by rapid cell death due to the cytopathic effect of OBP-401, as evidenced by floating, highly light-refractile cells under phase-contrast photomicrographs.

We also quantified GFP expression in human SCCHN cells following OBP-401 infection by using a fluorescence plate reader. Relative expression levels of GFP gradually increased in a dose-dependent manner (Fig. 2B). Moreover, we found an apparent inverse correlation between relative GFP expression at 72 h after OBP-401 infection and the ID_{50} values of OBP-301 in various human cancer cell lines including SCCHN cell lines (Fig. 2C), indicating that the outcome of OBP-301 treatment could be predicted by measuring GFP expression following OBP-401 infection.

In vivo *antitumor effect of intratumoral injection of OBP-301 in an orthotopic nude mouse model of human SCCHN.* To assess the effect of OBP-301 on SCCHN *in vivo*, we used an orthotopic animal model for SCCHN in which SAS-L cells were implanted into the tongues of BALB/c *nu/nu* mice. Histopathologic examination of the excised primary tumors showed a tumor formation composed of implanted SAS-L cells with a solid architecture (Fig. 3A). Mice bearing palpable SAS-L tumors with a diameter of 3 to 5 mm received three courses of intratumoral injections of 10^8 pfu of OBP-301 or PBS (mock treatment) every 3 days beginning on the 7th day (regimen 1) or 10th day (regimen 2) after the initial tumor inoculation (Fig. 3B). Representative images from each group showed that tumors treated with OBP-301 starting on day 7 after tumor inoculation were consistently smaller than those of mock-treated mice 28 days after the first viral injection (Fig. 3C).

Tumor growth at the primary site and body weight were continuously monitored. Intratumoral injection of OBP-301 in both regimens induced a gradual reduction in tumor volumes compared with mock-treated mice. Mice with tumor shrinkage significantly recovered body weight starting on day 10 (regimen 1) or day 15 (regimen 2) after the last virus injection ($P < 0.05$), although there was a decrease in body weight in the control group (Fig. 3D). This antitumor effect could be observed in mice orthotopically implanted with HSC-3 cells; the appearance of the effect, however, was ~4 to 5 days slower than that of SAS-L tumor-bearing mice (Supplementary Fig. S4).

Locoregional spread of virus following virotherapy in an orthotopic human SCCHN model. SCCHN patients with metastases to regional lymph nodes have a poorer prognosis than patients without nodal metastases (16). To verify whether adenoviruses could traffic to regional lymph nodes through the lymphatics, we injected 1×10^8 pfu of OBP-401 into SAS-L tumors implanted into the tongues of mice. Five days after virus injection, primary tongue tumors as well as lymph node metastases could be detected as light-emitting spots with GFP fluorescence under the optical charge-coupled device imaging (Fig. 5A). We also found that OBP-401 could infect and replicate in SAS-L cells trafficking in lymphatic vessels (Fig. 5B). These results suggest that although adenoviruses could effectively drain to regional lymph nodes, OBP-401 replicated only in metastatic lymph nodes, which was confirmed by a histopathologic analysis. Metastatic SCCHN cells were mostly observed in the lymph nodes with fluorescence emission, whereas most of GFP-negative lymph nodes contained no tumor cells (Fig. 5C). The optical imaging detected 13 lymph nodes labeled in spots with GFP fluorescence in 14 metastatic nodes (sensitivity of 92.9%). Among 21 metastasis-free lymph nodes, 3 nodes were GFP positive (specificity of 85.7%). In another orthotopic model implanted with HSC-3 human SCCHN cells, we could also detect GFP signals in one or two metastatic lymph nodes but not in other nonmetastatic nodes and salivary glands (Fig. 5; Supplementary Fig. S5).

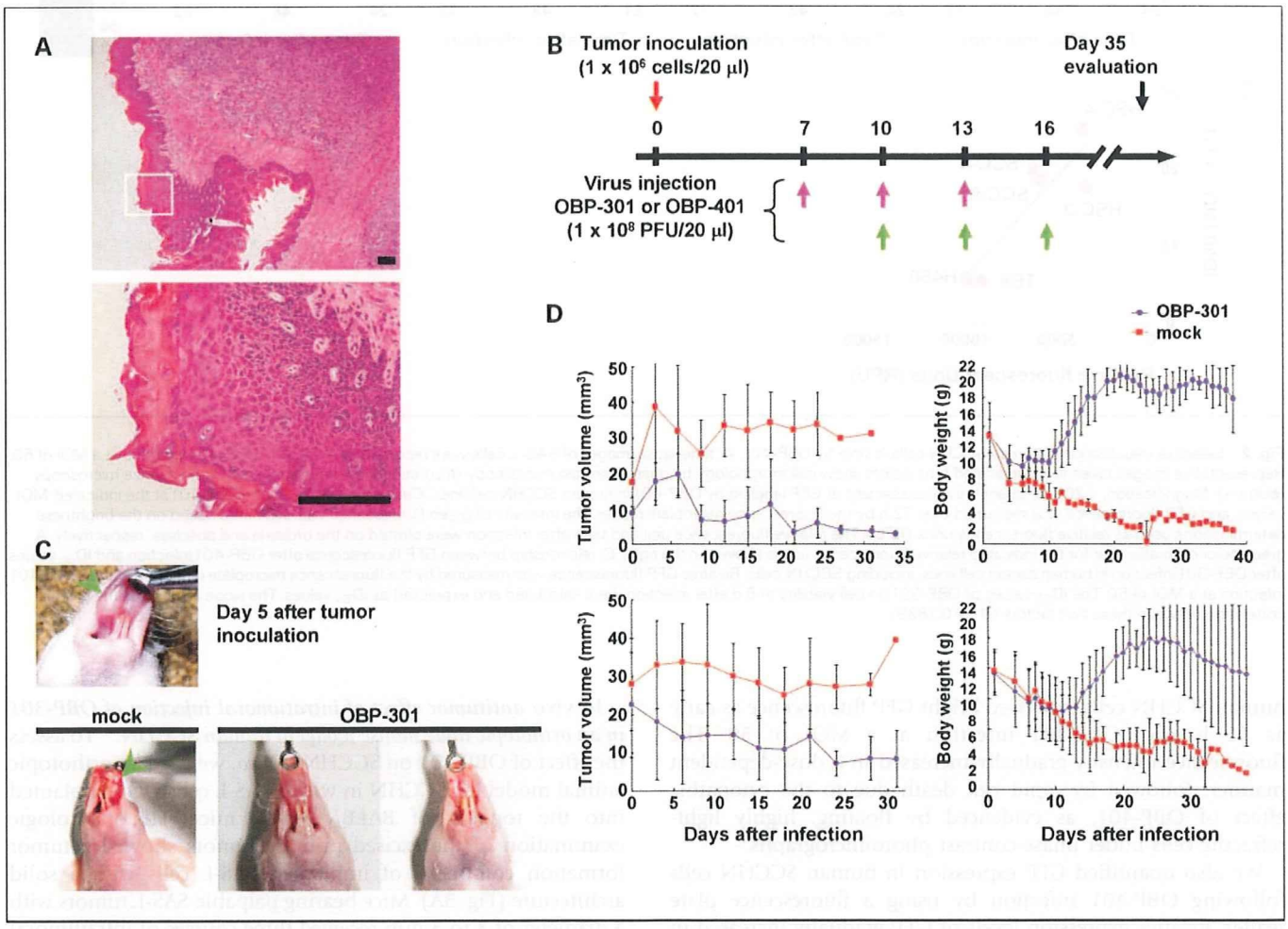

Fig. 3. Antitumor effects of OBP-301 *in vivo* in an orthotopic SCCHN model. *A,* tumor sections were obtained 35 d after tumor cell implantation. Paraffin-embedded sections of SAS-L tongue tumors were stained with H&E. Scale bar, 100 μm. Top, ×40 magnification; bottom, detail of the boxed region of the top panel; magnification, ×400. *B,* orthotopic animal experiment regimens. The tongues of BALB/c *nu/nu* mice were inoculated with 1×10^5 SAS-L human SCCHN cells. Orthotopic tumor-bearing mice received three courses of intratumoral injection of 1×10^8 pfu of viruses every 3 d starting on day 7 (regimen 1) or day 10 (regimen 2) after tumor cell inoculation. Eight mice were used in each group. *C,* macroscopic appearance of SAS-L tongue tumors on BALB/c *nu/nu* mice 5 d (*top*) or 35 d (*bottom*) after tumor cell inoculation. Representative tumors treated with PBS or OBP-301 are shown. Note the eradicated tumors in mice that received OBP-301 injection. Green arrowhead, SAS-L tumors. *D,* orthotopic tumor-bearing mice received three courses of intratumoral injection of 1×10^8 pfu of viruses every 3 d starting on day 7 (regimen 1; *top*) or day 10 (regimen 2; *bottom*) after tumor cell inoculation. The tumor volume (*left*) and the body weight (*right*) were monitored and plotted. Point, mean; bars, SD. Statistical significance was defined as $P < 0.05$.

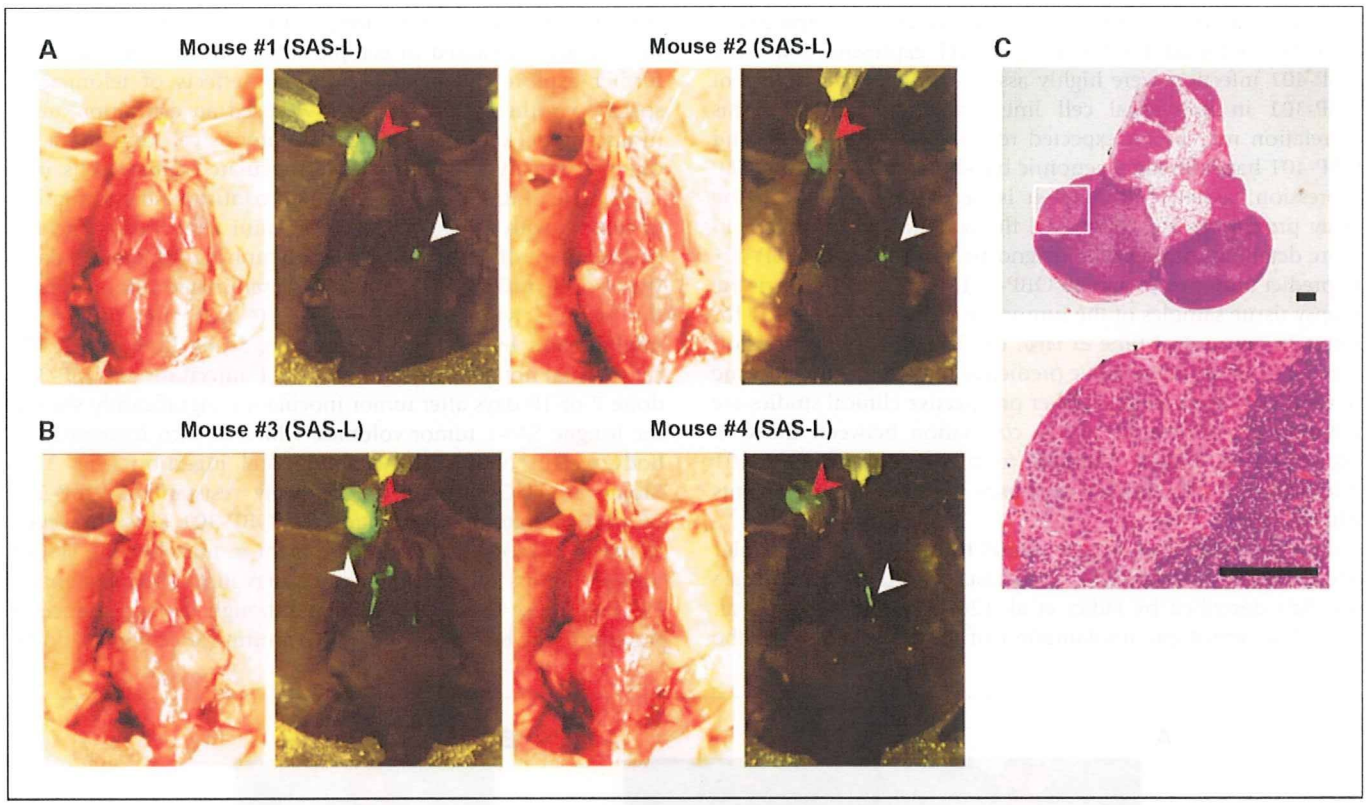

Fig. 4. Virus spread of OBP-401 via lymphatics to regional lymph nodes on SAS-L tumor-bearing mice. *A*, selective visualization of lymph node metastasis in orthotopic xenografts of SAS-L human SCCHN cells. Mice received intratumoral injection of OBP-401 (1×10^8 pfu) 24 d after tumor inoculation and were assessed for lymph node metastasis 5 d later under charge-coupled device imaging. Left, gross appearance; right, fluorescence image. Red arrowhead, primary tumor; white arrowhead, metastatic tumor cells. *B*, selective visualization of lymph node metastasis and lymphatic dissemination in orthotopic xenografts of SAS-L cells. Note the GFP-expressing disseminated tumor cells in lymphatics. Red arrowhead, primary tumor; white arrowhead, metastatic tumor cells in lymphatics. *C*, sections of GFP-positive lymph nodes were obtained 35 d after tumor cell implantation. Paraffin-embedded sections of lymph nodes were stained with H&E. Scale bar, 100 μm.

Prolonged survival following OBP-301 virotherapy in an orthotopic human SCCHN model. Finally, we assessed the effect of intratumoral injection of OBP-301 on survival time of SAS-L–bearing mice. Mice treated with OBP-301 beginning either on the 7th day (regimen 1) or the 10th day (regimen 2) after tumor implantation survived significantly longer (mean = 27.4 or 33.7 days) than mice without treatment (mean = 14.7 or 24.3 days; regimen 1, $P = 0.017$; regimen 2, $P = 0.016$; Fig. 6). The prolonged survival might reflect an antitumor effect of oncolytic adenoviruses spreading into the locoregional area, including regional lymph nodes.

Discussion

The present study illustrates the potential application of replication-selective oncolytic adenoviruses as an anticancer agent in human SCCHN patients. We found that intratumoral administration of telomerase-specific oncolytic adenovirus induced tumor volume reduction as well as the recovery of weight loss by enabling oral ingestion in an orthotopic xenograft model, in which human SCCHN cells were implanted into the tongues of BALB/c *nu/nu* mice. Oncolytic virotherapy also prolonged the survival of SCCHN tumor-bearing mice, presumably due to the locoregional antitumor effect against primary tumors and lymph node metastases with viruses spreading into the lymphatics.

Telomerase-specific oncolytic adenovirus OBP-301 exhibits a broad cytopathic effect against human cancer cell lines of different tissue origins (8–10). In a panel of human SCCHN cell lines, OBP-301 also showed apparent antitumor effects *in vitro* in a dose-dependent manner (Fig. 1B), although the sensitivity varied greatly between cell lines despite hTERT and coxsackievirus and adenovirus receptor expression (Supplementary Fig. S1). We have previously found that the process of oncolysis is morphologically distinct from apoptosis and necrosis (17). The cell death machinery triggered by OBP-301 infection is still under the investigation, although autophagy is partially involved in this effect (17, 18). OBP-301 has been developed based on the ability of the hTERT promoter to control replication of the virus in the tumors, leading to selective killing of tumor cells and minimal undesired effects on normal cells; the ID_{50} values of OBP-301 in various human cancer cell lines, however, were not related to the levels of *hTERT* mRNA expression (8, 10). Indeed, HSC-3 and HSC-4 human SCCHN cells expressing high levels of *hTERT* mRNA were less sensitive to OBP-301 than SCC-4 and SCC-9 cells with low levels of hTERT expression. Thus, neither hTERT expression nor coxsackievirus and adenovirus receptor expression could be useful for predicting the outcome of OBP-301 treatment.

Biomarkers have been extensively studied and often used to predict the potential therapeutic benefit of new agents, including molecular-targeted therapies (19). There is a widely recognized need for biomarkers that could improve the

clinician's ability to select suitable drugs for appropriate patients. We found that the levels of GFP expression following OBP-401 infection were highly associated with ID_{50} values of OBP-301 in individual cell lines *in vitro* (Fig. 2C). This correlation may be an expected result, because OBP-301 and OBP-401 have the same genomic backbone except for the GFP expression cassette. Although it is necessary to establish the assay procedures for GFP-based fluorescence measurement in more detail, we propose the diagnostic application of OBP-401 to predict tumor responses to OBP-301. For example, when the biopsy tissue samples of the tumor are exposed to OBP-401 for a certain amount of time *ex vivo*, the levels of GFP expression may be of value as a positive predictive marker for the outcome of OBP-301 virotherapy. Further prospective clinical studies are required to confirm the direct correlation between the GFP expression in biopsy samples following *ex vivo* OBP-401 infection and the clinical responses to OBP-301 in patients with SCCHN.

An orthotopic nude mouse model to investigate the cellular and molecular mechanisms of metastasis in human neoplasia was first described by Fidler et al. (20, 21) and Killion et al. (22). The orthotopic implantation of tumor cells restores the correct tumor-host interactions, which do not occur when tumors are implanted in ectopic subcutaneous sites (20). To further explore the *in vivo* antitumor effects of telomerase-specific virotherapy for SCCHN, we used an orthotopic nude mouse model of human tongue squamous cell carcinoma. In our preliminary experiments, we inoculated tumor cells into the tongue of BALB/c *nu/nu* mice and confirmed the formation of tumors with a diameter of 3 to 5 mm after 5 days and the development of metastases in neck lymph nodes after 35 days. We also identified the presence of disseminated tumor cells in the regional lymph nodes at least 10 days after tumor cell implantation by using GFP-expressing SAS-L human SCCHN cells (data not shown). Intratumoral injection of OBP-301 done 7 or 10 days after tumor inoculation significantly shrunk the tongue SAS-L tumor volumes, which in turn increased the body weight of mice by enabling oral ingestion (Fig. 3D). Moreover, HSC-3 cells were relatively resistant to OBP-301 *in vitro*; intratumoral injection of OBP-301 was, however, effective for recovering the body weight in mice bearing HSC-3 tongue tumors after a long-term observation (Supplementary Fig. S4). These results suggest that although the appearance of the effect may be slower, the *in vivo* antitumor activity could be

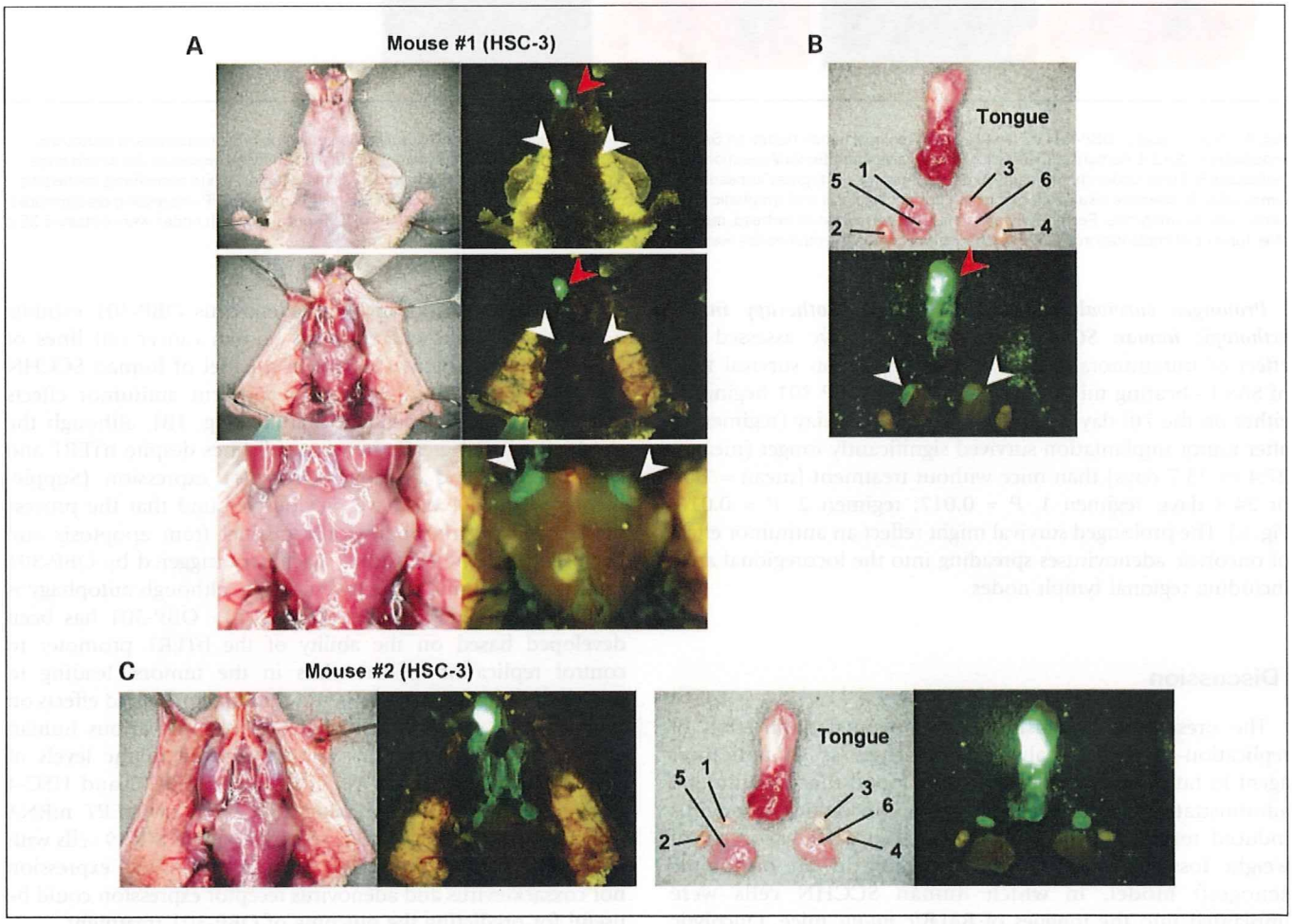

Fig. 5. Virus spread of OBP-401 via lymphatics to regional lymph nodes on HSC-3 tumor-bearing mice. *A*, selective visualization of lymph node metastasis in orthotopic xenografts of HSC-3 human SCCHN cells. Mice received intratumoral injection of OBP-401 at the concentration of 1×10^8 pfu after 24 d of tumor inoculation and were assessed for lymph node metastasis 5 d later under fluorescence stereomicroscope. *B*, HSC-3 primary tumor, salivary glands, and lymph nodes were excised 5 d after OBP-401 injection and then assessed for GFP fluorescence. 1 to 4, lymph nodes; 5 and 6, salivary glands. *C*, other HSC-3 tumor-bearing mice. Excised primary tumors, salivary glands, and lymph nodes were assessed for GFP fluorescence.

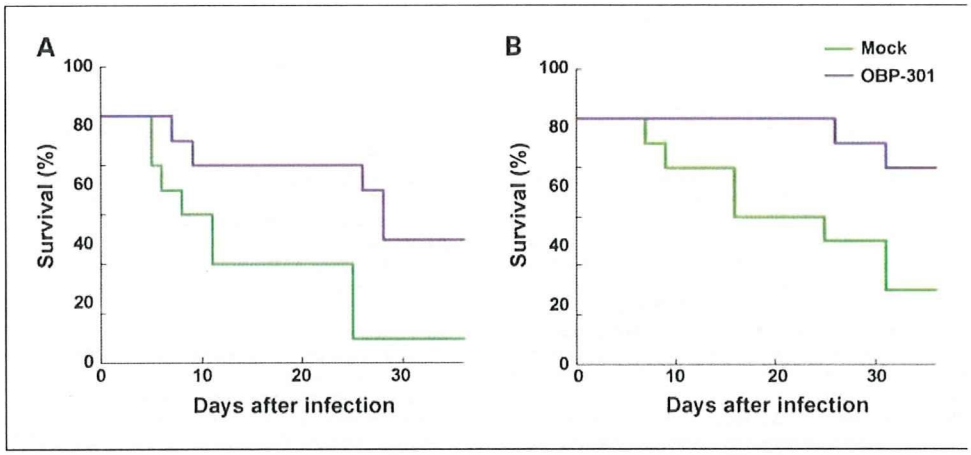

Fig. 6. Prolonged survival of SAS-L tumor-bearing mice treated with OBP-301. Mice bearing SAS-L xenografts were treated starting on day 7 (regimen 1; *A*) or day 10 (regimen 2; *B*) after tumor cell inoculation as described in Fig. 3A. Survival was monitored over time after virus injection and plotted as a Kaplan-Meier plot.

expected even in resistant SCCHN tumors. Because the body weight loss due to a feeding problem in this orthotopic SCCHN model resembles the disease progression in SCCHN patients, the finding that OBP-301 increased the body weight of mice suggests that OBP-301 virotherapy could potentially improve the quality of life in advanced SCCHN patients.

Amplified viruses can infect adjacent tumor cells as well as reach metastatic lymph nodes via the lymphatic circulation. We have previously shown that the telomerese-specific OBP-401–expressing GFP could be delivered into human tumor cells in regional lymph nodes and replicate with selective GFP fluorescence after injection into the primary tumor in an orthotopic rectal tumor model (11). In the orthotopic SCCHN model, OBP-401 spread into the neck lymph nodes after injection into the primary tongue tumor and selectively replicated in metastatic nodules (Figs. 4 and 5; Supplementary Fig. S5). The sensitivity and specificity of this imaging strategy for SAS-L tumors are 92.9% and 85.7%, respectively, which are sufficiently reliable to support the concept of this approach. These results suggest that surgeons may be able to excise primary tumors as well as metastatic lymph nodes precisely with appropriate margins by using this novel surgical navigation system with OBP-401. Moreover, the therapeutic profiles of OBP-401 and OBP-301 are considered similar, and a histopathologic analysis showed the destruction of micrometastases by virus in metastatic lymph nodes. This regional antitumor effect of oncolytic viruses could have a significant effect on the prolongation of the survival of mice bearing orthotopic tumors (Fig. 6).

Targeted therapies such as the anti–epidermal growth factor receptor monoclonal antibody cetuximab and other small-molecule epidermal growth factor receptor–tyrosine kinase inhibitors have been developed for SCCHN. Although a phase III trial showed a survival benefit with cetuximab and standard platinum-based therapy in SCCHN patients (23), some patients are exquisitely sensitive to these drugs and can develop particular and severe toxicities (24). A phase I study is currently under way in the United States to determine the feasibility and to characterize the pharmacokinetics of OBP-301 in patients with histologically proven nonresectable solid tumors (25). An interim analysis of the first 12 patients, including four SCCHN patients treated with escalating doses of OBP-301, indicates that OBP-301 virotherapy is well tolerated without any severe adverse events, suggesting that OBP-301 may be much more potent than other targeted therapies for human SCCHN in terms of specificity, efficacy, and toxicity.

In conclusion, our data clearly indicate that telomerase-specific oncolytic adenoviruses have a significant therapeutic potential against human SCCHN *in vitro* and *in vivo*. Moreover, these viruses can be used in an *ex vivo* diagnostic assay to predict the therapeutic potential of the virus in SCCHN patients. The combination of a diagnostic assay with a therapeutic entity is termed theranostics (26). Telomerase-specific oncolytic viruses can be used to treat the patients and to identify the patients who will likely benefit from virotherapy (Supplementary Fig. S6). In addition, telomerase-specific *in situ* imaging strategy has a potential of being widely available in humans as a navigation system in the surgical treatment of SCCHN. Thus, our oncolytic virus–based approach might be a novel "virotheranostics" for SCCHN. Phase II studies of telomerase-specific virotheranostics in advanced SCCHN patients are warranted.

Disclosure of Potential Conflicts of Interest

H. Onimatsu and Y. Urata are employed by Oncolys BioPharma, Inc. T. Fujiwara is a consultant to Oncolys Biopharma, Inc.

Acknowledgments

We thank Daiju Ichimaru and Hitoshi Kawamura for their helpful discussions and Tomoko Sueishi for her excellent technical support.

References

1. Parkin DM, Bray F, Ferlay J, Pisani P. Global cancer statistics, 2002. CA Cancer J Clin 2005;55:74–108.
2. Jemal A, Clegg LX,Ward E, et al. Annual report to the nation on the status of cancer, 1975–2001, with a special feature regarding survival. Cancer 2004;101:3–27.
3. Vokes EE, Weichselbaum RR, Lippman SM, Hong WK. Head and neck cancer. N Engl J Med 1993;328:184–94.
4. Vokes EE, Crawford J, Bogart J, Socinski MA, Clamon G, Green MR. Concurrent chemoradiotherapy for unresectable stage III non-small cell lung cancer. Clin Cancer Res 2005;11:5045–50s.
5. Milas L, Mason KA, Liao Z, Ang KK. Chemoradiotherapy: emerging treatment improvement strategies. Head Neck 2003;25:152–67.
6. Kirn D, Martuza RL, Zwiebel J. Replication-selective virotherapy for cancer: biological principles, risk management and future directions. Nat Med 2001;7:781–7.
7. Hawkins LK, Lemoine NR, Kirn D. Oncolytic